ALMA MATER STUDIORUM
UNIVERSITA' DI BOLOGNA

SCUOLA DI INGEGNERIA ED ARCHITETTURA
-Sede di Forlì-

CORSO DI LAUREA
IN INGEGNERIA AEROSPAZIALE
Cod. 8197

TESI DI LAUREA
in Tolleranza al Danno di Strutture Aeronautiche LM

Investigation on Laser Shock Peening Capability by FE Simulation

CANDIDATO
Cinzia Crudo

RELATORE
Prof. Ing. Enrico Troiani

CORRELATORE
Dott. Ing. Domenico Furfari

Anno accademico 2012-2013
Sessione I

"The most effective way to do it,

is to do it"

(Amelia Earhart)

Index

Table of Figures

Table of Tables

Abbreviations

BC	Boundary Condition
BCC	Body Centered Cubic
C3D83	8-node linear brick element, reduced integration with hourglass control
EOS	Equation of State
EPP	Elastic perfectly plastic
FCC	Face Centered Cubic
FE	Finite Element
FEM	Finite Element Method
FOD	Foreign Object Damage
FWHM	Full Width at Half Maximum
GE	General Electrics
HCF	High Cycle Fatigue
HEL	Hugoniot Elastic Limit
ICHD	Incremental Centre Hole Drilling
JC	Johnson Cook
LBV	Linear Bulk Viscosity
LCF	Low Cycle Fatigue
LPB	Low Plasticity Burnishing
LPwC	Laser Peening without Coating
LSP	Laser Shock Peening
MIC	Metal Improvement Company
MIC	Metal Improvement Company
QBV	Quadratic Bulk Viscosity
USP	Ultrasonic Peening
WFM	Weight Function Method
XRD	X-Ray diffraction
ZA	Zerilli-Armstrong

Abstract

Laser shock peening is a technique similar to shot peening that imparts compressive residual stresses in materials for improving fatigue resistance.
The ability to use a high energy laser pulse to generate shock waves, inducing a compressive residual stress field in metallic materials, has applications in multiple fields such as turbo-machinery, airframe structures, and medical appliances.
The transient nature of the LSP phenomenon and the high rate of the laser's dynamic make real time in-situ measurement of laser/material interaction very challenging.
For this reason and for the high cost of the experimental tests, reliable analytical methods for predicting detailed effects of LSP are needed to understand the potential of the process.
Aim of this work has been the prediction of residual stress field after Laser Peening process by means of Finite Element Modeling.
The work has been carried out in the Stress Methods department of Airbus Operations GmbH (Hamburg) and it includes investigation on compressive residual stresses induced by Laser Shock Peening, study on mesh sensitivity, optimization and tuning of the model by using physical and numerical parameters, validation of the model by comparing it with experimental results.
The model has been realized with Abaqus/Explicit commercial software starting from considerations done on previous works.
FE analyses are “Mesh Sensitive”: by increasing the number of elements and by decreasing their size, the software is able to probe even the details of the real phenomenon. However, these details, could be only an amplification of real phenomenon. For this reason it was necessary to optimize the mesh elements' size and number.
A new model has been created with a more fine mesh in the trough thickness direction because it is the most involved in the process deformations.

This increment of the global number of elements has been paid with an "in plane" size reduction of the elements far from the peened area in order to avoid too high computational costs.

Efficiency and stability of the analyses has been improved by using bulk viscosity coefficients, a merely numerical parameter available in Abaqus/Explicit.

A plastic rate sensitivity study has been also carried out and a new set of Johnson Cook's model coefficient has been chosen.

These investigations led to a more controllable and reliable model, valid even for more complex geometries.

Moreover the study about the material properties highlighted a gap of the model about the simulation of the surface conditions.

Modeling of the ablative layer employed during the real process has been used to fill this gap.

In the real process ablative layer is a super thin sheet of pure aluminum stuck on the masterpiece.

In the simulation it has been simply reproduced as a 100μm layer made by a material with a yield point of 10MPa.

All those new settings has been applied to a set of analyses made with different geometry models to verify the robustness of the model.

The calibration of the model with the experimental results was based on stress and displacement measurements carried out on the surface and in depth as well.

The good correlation between the simulation and experimental tests results proved this model to be reliable.

Chapter 1

1. Fatigue and residual stresses in aeronautical structures

1.1 Introduction

The primary objective of the aerospace industry is to offer products that not only meet the operating criteria in terms of payloads and range but also significantly reduce the direct operating costs of their customers, the airlines. The structure of the present civil transport aircraft is designed considering the current and forthcoming airworthiness regulations, the customers´ requirements and manufacturing aspects.[1]

Among the design processes that affect aircraft structural integrity, fatigue is a very important area of concern.

Tab. 1-1 shows some design criteria for aeronautical structures.

Mode of failure	Design criteria	Design allowable
1. Static strength of undamaged structure	Structure must support Ultimate Loads (UL) without failure for 3 seconds	Static properties
2. Deformation of undamaged structure	• No permanent deformation below Limit Loads (LL) and • deformation of undamaged structure at limit loads may not interfere with safe operation	Static properties and creep properties for elevated temperature conditions
3. Fatigue crack initiation of undamaged structure	• Damage tolerant structure must meet service life requirements • Safe life components must remain crack free in service	Fatigue properties
4. Crack growth life of damaged structure	For damage tolerant structure inspection techniques and frequency must be specified to minimise risk of catastrophic failures	Crack growth properties and Fracture toughness properties
5. Residual static strength of damaged structure	Damaged structure must support limit loads without catastrophic failure	Static properties and Fracture toughness properties

Fatigue and Damage Tolerance [F&DT] Design Criteria

Tab. 1-1 Fatigue and Damage Tolerance Design Criteria [2]

1.2 Fatigue design Overview

Fatigue is a process of progressive permanent structural material damage when a component is subjected to repeated cyclic stresses associated with operating loads. Therefore it is a failure mode that occurs as a result of large number of load fluctuations. A single load cycle will not hurt the material or the structure if the load is below the static failure load. However if the load is repeated many times a fatigue failure can occur. [3]

The history of engineering structures has been marked by several fatigue failures, however the connection between the cyclic loading and the failure was noted only in 19st century, when for the first time the failure mechanism was named "material fatigue". In this period noteworthy engineering research and experimental works were done by August Wöhler who was investigating the fatigue failure in railroad axles for the German Railway Industry.

Since then an enormous amount of research has been done on fatigue and an historical overview covering a time span from 1837 to 1994 can be found in [4].

In particular, in the Aeronautic world, the happening of serious accidents caused by fatigue failure influenced the development of new design methods.

These case histories and their influences on aircraft structural integrity can be found in the following Tab.1-2.

year	*aircraft failure*	*influence, follow-up*
1954	DeHavilland Comet; two aircraft crashed owing to fuselage explosions.	General awareness of finite aircraft fatigue life as an important issue for passenger safety. Attention drawn to full-scale fatigue testing.
1969	F-111; wing failure due to undetected material flaw.	Aircraft should be damage tolerant. Fatigue cracking due to initial damage should be considered.
1977	Boeing 707; tailplane lost owing to fatigue failure in spar.	Old aircraft become more fatigue-critical, *geriatric aircraft*.
1988	Boeing 737; aircraft lost part of fuselage skin structure owing to multiple fatigue cracks in spar splices.	Multiple Site fatigue Damage (MSD) can occur in *ageing aircraft*, especially in lap joints of the pressurized structure.

Tab. 1-2 Milestone case histories in aircraft structural integrity [5]

Considerations raised up from the above mentioned accidents led to formally outline new design approaches that could take into account fatigue failures.

An overview of those design developments for civil and military aircrafts can be found in Tab.1-3.

Accidents	Design developments	
1950s 1954 Comet fuselage failures - design details ;stress concentrations **1960s** **1969** F111 wing pivot failure-manufacturing defects **1970s** **1976** H-S748 wing failure **1977** B 707 stabiliser **1979** DC10 Chicago **1980s** **1988:** Aloha airlines loses most of upper fuselage in flight due to widespread and multiple site fatigue damage **1990s**	**Civil aircraft** Safe Life **1959**: first directives on fail safe aircraft design Safe life design continues as an option together with fail safe **1980** recommendations for damage Tolerance for large civil aircraft **1978, 1981** Introduction of supplemental inspections for ageing aircraft **Post 1988** Major investigations and recommendations for inspection, maintenance and repair of ageing aircraft Continued investigations into ageing aircraft fatigue, corrosion and fracture behaviour **1990s** Gradual elimination of safe life parts from large civil aircraft, In 2005, only the Undercarriage and engines remain Safe life Attempts to require that civil helicopters become damage tolerant	**Military Aircraft** Safe Life Safe life continues as an option **1974:** MIL A-83444 Damage tolerance plus fail- safe for USAF; Europe continues with Safe life Cranfield UNIVERSITY

Tab. 1-3 Summary of Accidents and design developments for civil and military aircrafts [3]

The above mentioned design philosophies can be summarized in three main approaches.

- Safe Life approach. Is the first design philosophy developed in early 1950s, sometimes called also "finite life". With this approach, in fact, the structure is supposed to be crack free and the estimation of the whole life of an aircraft is to be based on the component with lowest fatigue life.

- Fail safe approach. This design philosophy arose in late 1950s after the Comet accident happened in 1954. The design assumption is that failure will eventually occur but when it does the device, system or process will fail in a safe manner. In other words, with this philosophy, an aircraft is designed to have an adequate life free from damage but operation is permitted even beyond the life at which such damage may develop. This is usually obtained by applying redundancy of structural members and granting load transfer capability.
- Damage tolerance approach. This concept was introduced in late 1970s to ensure aircraft structural integrity. The fundamental difference from the other approaches is that, with this philosophy small cracks and flaws are supposed to be already present in the structures as manufactured and they can propagate during the operating life. To implement the damage tolerance concept it is therefore essential to clearly define parameters like initial crack lengths and inspection periods. Components must be accessible for inspections without dismantling and an accurate inspection plan must be assessed. Moreover crack growth rate and residual strength in the presence of long cracks calculations are needed.

  Another key-point of this philosophy is the opportunity to consider crack arrest or retardation and the related strategy to realize them, like, for example, application of compressive residual stresses.

  This approach is currently used in civil aircrafts' design.

1.3 Residual stresses

Residual stresses (RS) are those which remains in a body that is stationary and at equilibrium with its surroundings.

They can be either compressive or tensile in nature but compressive stresses are sometimes introduced deliberately to improve fatigue resistance.

As the design of engineering components becomes less conservative, there is an increasing interest in how residual stress affects mechanical properties. This is because structural failure can be caused by the combined effect of residual and applied stresses. In practice, it is not likely that any manufactured component would be entirely free from residual stresses introduced during processing. Furthermore, in natural or artificial multiphase materials, residual stresses can arise from differences in thermal expansivity, yield stress, or stiffness.

Considerable effort is currently being devoted to the development of a basic framework within which residual stresses can be incorporated into design in aerospace, nuclear, and other critical engineering industries [6][7].

Depending on the scale over which they equilibrate, residual stresses are categorized into three different types [8].

.

Type I- Macroscopic Stresses, which are homogeneous over a length scale representative of the dimension of the material or component and the net forces due to these stresses is balanced over the same scale length.

Type II - Intergranular stresses exist at the grain scale, and are generally present to some extent in all polycrystalline materials. This type of stress appears in the structure due to inhomogeneous plastic flow or thermal mismatch at the grain level, or the presence of more than one phase (precipitates) or phase transformation in the structure.

Type III- Atomic stresses exist over atomic dimensions and balance within a length scale comparable with the grain size. Examples of these stresses are those caused by dislocations and point defects [7].

They are shown in Fig.1-1 where the process (source of RS) is shown on the left, the misfit in the centre and corresponding residual stress on the right hand side for each case.

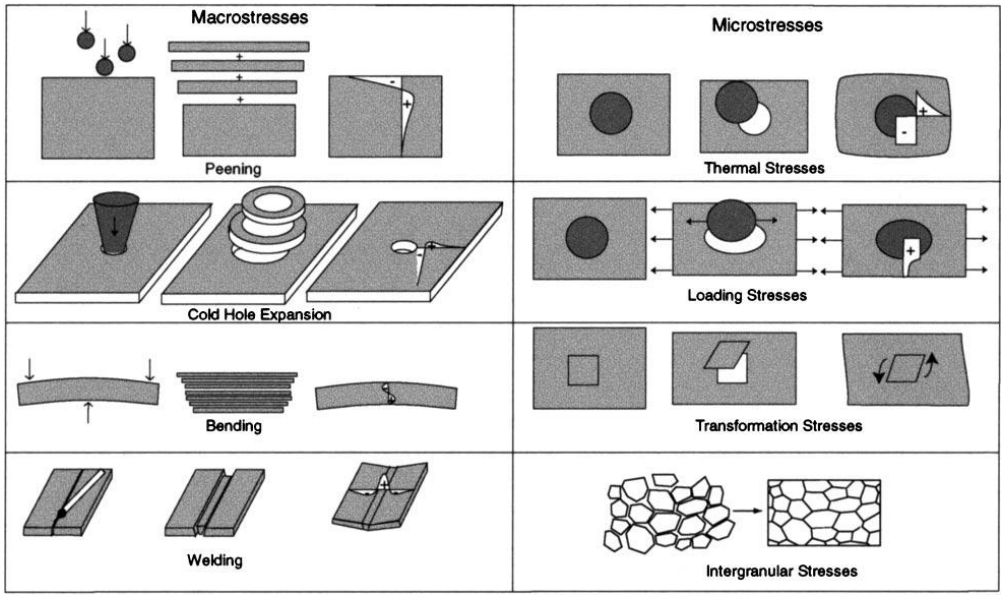

Figure 1-1 Schematic representation of different type of residual macro and microstresses [6]

As already mentioned, many processing techniques introduce a significant amount of residual stress in the structure. Moreover, when these components are in use these existing residual stresses can be modified or new stresses can be created locally. The new state of the stresses interacts with the existing micro-cracks modifying their crack growth process and, in the worst case, leading to premature or sometimes catastrophic failure of the parts.

1.3.1 Effect of residual stresses on crack growth

As already mentioned in §1.2 fatigue damages arose in those components subjected to repeated cyclic stresses.

Cyclic stresses resulting from constant or variable amplitude loading can be described by two of a number of alternative parameters.

If we consider, for example, constant amplitude cyclic stresses (as in Fig.1-2), they can be defined by three parameters: a mean stress σ_m , a stress amplitude σ_a , and a period T (i.e the inverse of the frequency). This last parameter is not however needed to describe the magnitude of the stresses, so just two parameters are sufficient.

It is also possible to use other parameters like the maximum stress σ_{max} or the minimum one σ_{min} or simply the stress range $\Delta\sigma = \sigma_{max} - \sigma_{min}$.
Another important parameter is $R = \sigma_{min}/\sigma_{max}$, called stress ratio, that can replace one of the others above mentioned.
The number of those cycle is usually expressed by letter *N*.

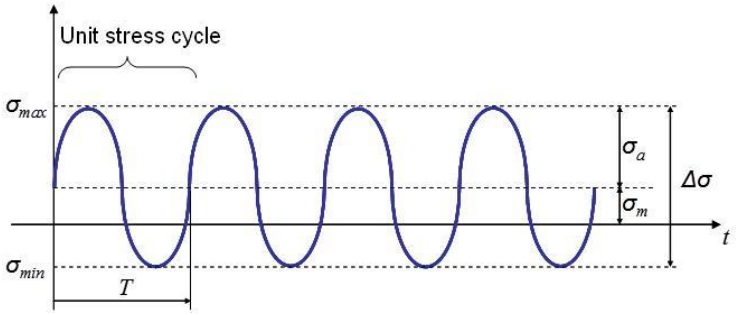

Figure 1-2 Constant amplitude stress cycle

The crack growth mechanism shows that a fatigue crack grows by a minute amount in every load cycle; the mechanism is schematically shown in the Fig.1-3 beside. Growth is the geometrical consequence of slip and crack tip blunting. Resharpening of the crack tip upon unloading, sets the stage for growth in the next cycle.
The crack growth per cycle, indicated by *Δa*, will be larger if the maximum stress in the cycle is higher (more opening) and if the minimum stress is lower (more resharpening).

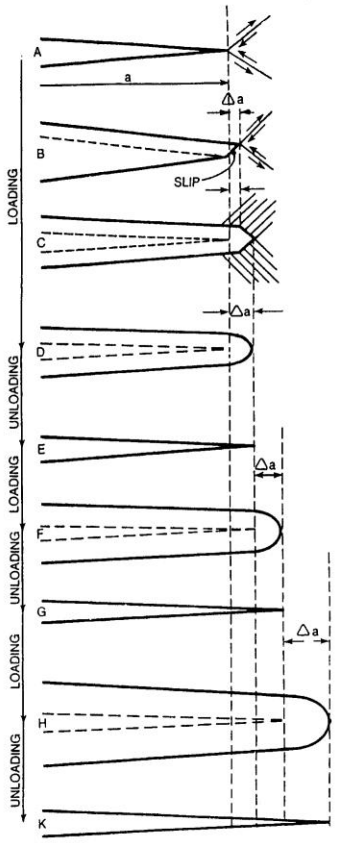

Figure 1-3 Crack growth schematic mechanism [9]

The most simple representation of a crack growth record is a graph with the crack length data plotted as a function of the number of cycles (Fig.1-4)
Two different typical curves are shown, for high and slow stress amplitudes, while the initial crack length is supposed for both equal to $a_{0.}$

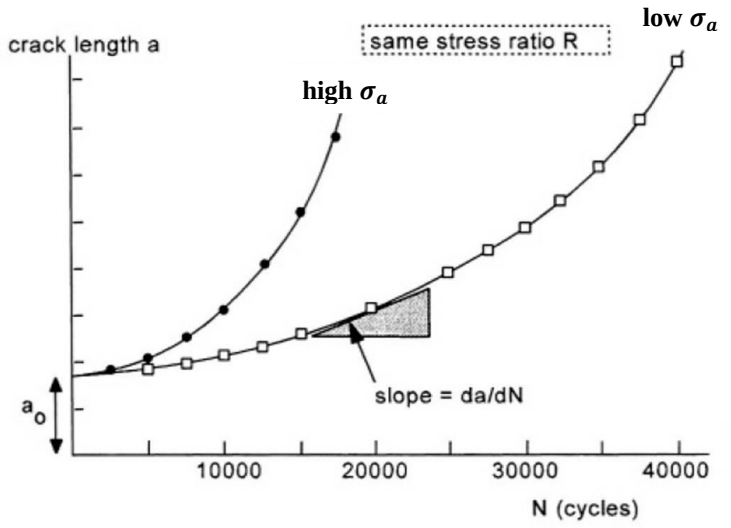

Figure 1-4 a-N curve for high and low stress amplitudes [5]

The slope of a crack growth curve is the crack growth rate indicated by da/dN , it can be plotted (as in Fig.1-5) as a function of the crack length for high and lox stress amplitudes, as well.

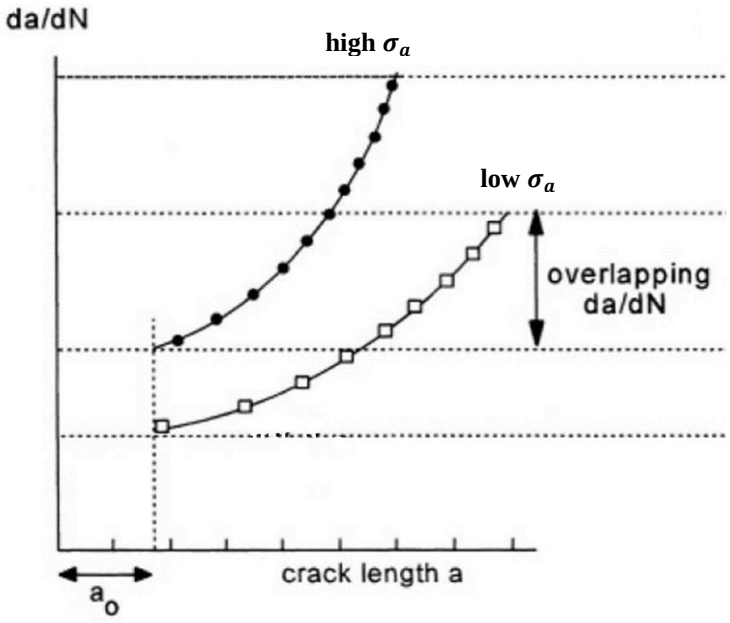

Figure 1-5 Fatigue crack growth for high and low stress amplitudes [5]

As shown in fig.1-5 there is an interval in which crack growth rates for both high and low stress amplitudes are partly overlapping, although for different values of crack length.

This kind of similarity is perfectly expressed by Paris law that put in relation crack growth rate with a characteristic parameter *K*, called stress intensity factor, by two other constant *C* and *n*, as follow:

$$\frac{da}{dN} = C(\Delta K)^n \tag{1.1}$$

The stress intensity factor *K* is a parameter indicating the severity of the stress distribution around the tip of a crack.

If the cyclic stress varies in a load cycle with a stress range $\Delta\sigma$ then ΔK can be evaluated by the following:

$$\Delta K = \beta \Delta\sigma \sqrt{\pi a} \tag{1.2}$$

where β represents a geometric factor and $\Delta\sigma$ is the stress range as defined above.

Crack growth rate behavior can be plotted as in Fig.1-6 where region I, usually called *threshold* region, represents the stress intensity range ΔK_{th} below which no crack propagation occur. In region II crack grows linearly with the applied stress intensity factor range and eq. 1.1 holds. Once the applied ΔK reaches the critical stress intensity factor ΔK_C of the material, crack propagation occurs at a very fast rate and this is represented as region III.

The threshold value ΔK_{th} is associated with the growth of macro-cracks, i.e. fatigue cracks which have grown to a macroscopic size at ΔK level above ΔK_{th}. If ΔK is then decreased crack growth slows down and is assumed that no further grows occurs.

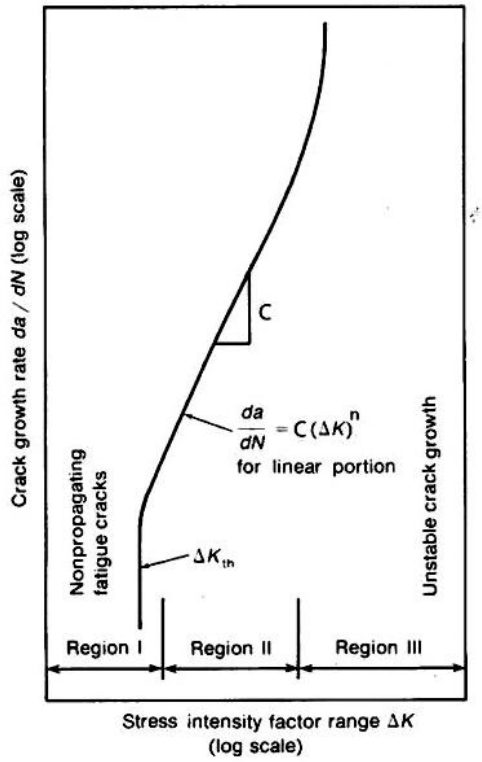

Figure 1-6 Schematic illustration of the three stages of fatigue crack growth [10]

Is therefore obvious that to improve crack growth behavior, and subsequently fatigue life, it is necessary to have low ΔK values.

This is possible, evidently from eq. 1.2, reducing $\Delta\sigma$ for example in one of the ways represented in Fig.1-7.

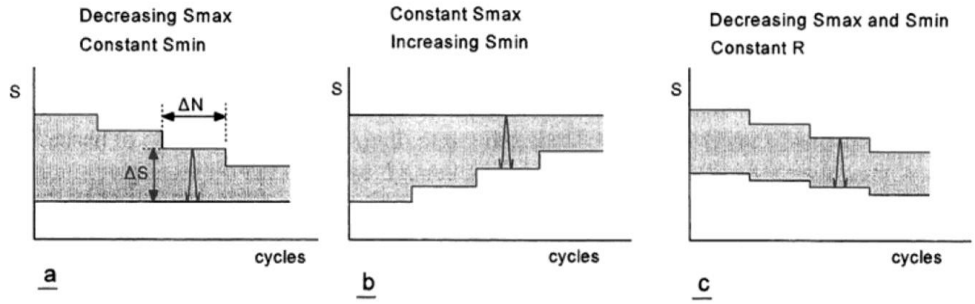

Figure 1-7 Different ways to reduce range stress [5]

This is exactly what residual stresses do in a load cycle. It must be, in fact, remembered that residual stresses are superimposed stresses onto the applied stress to give an effective stress intensity factor.

This is schematically represented in Fig.1-8 where profile *ii* represents the applied load cycle where no residual stresses are present in the structure. When a tensile residual stress field is superimposed onto the applied stress, the effective stress intensity factor becomes higher (profile *iii*). On the other hand, compressive residual stresses reduce the applied load and hence the stress intensity factor becomes lower (profile *iii*). Since negative stress intensity factors do not physically exist, only the positive part of the cycle is taken into account.

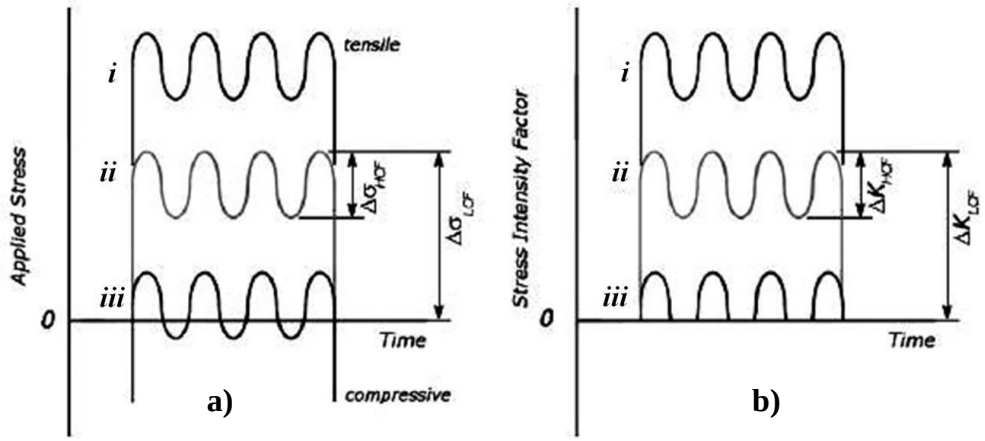

Figure 1-8 Influence of (a) residual stress on the total stress and (b) stress intensity factor under combined cycle. [11]

From those considerations a new value of the effective ΔK acts on the structure and it is equivalent to the sum of the applied ΔK and the K related to the residual stresses. Formally :

$$\Delta K_{eff} = \Delta K_{app} + K_{res} \tag{1.3}$$

Estimating K_{res} is not trivial and lot of studies on it are available in literature. The most common ways to evaluate this parameter are the *weight function method* (WFM) and finite element analyses.

Determination of K_{res} goes however beyond the objectives of this thesis that are confined to the determination of the global amount of residual stresses imparted on components by applying a particular surface treatment.

1.3.2 Residual stress imparting methods

There are at least four ways in which macro residual stresses can arise in engineering components: through the interaction between misfitting parts within an assembly, and through the generation of chemical, thermal, and plastically induced misfits between different regions within one part.

As already said, unintentional tensile residual stress can have ab adverse effect on the fatigue resistance, while compressive residual stress can significantly improve fatigue behavior. In this section it will be considered therefore only methods that can introduce compressive, and so beneficial, residual stresses.

Typically residual stresses can arise by one of three principal mechanisms: chemical treatments, heat treatments or mechanical processes.

1.3.2.1 Chemical treatments

Residual stresses obtained by chemical treatments develop due to volume changes associated with chemical reactions, precipitation or phase transformations.

The principal chemical treatments which are used to provide components with surface residual stress layers favorable to subsequent service fatigue loading conditions are nitriding, tufftriding and carburizing.

In all these cases a chemical component (nitrogen, carbon or both) is diffused on the superficial layer of the component creating a case hardened surface

1.3.2.2 Heat treatments

Unlike chemical treatments, heat treatment procedures do not alter the chemical composition at the surface but simply modify the metallurgical structure of the parent material.

Principal heat treatment procedures which induce favourable residual stress layers are induction hardening and flame hardening.

The principle of these treatments is the same of the quench: the component is subjected to an abrupt temperature step passing from very high to very low temperature.

Cooling usually occurs very fast in the external part of the component while the core is cooled down more slowly. The inhomogeneous cooling produce hence thermal residual stresses.

1.3.2.3 Mechanical Processes

The most significant mechanical processes which induce surface residual stresses are those which involve plastic yielding and hence “cold-working” of the material.

The plastic deformation causes dislocation movements responsible of the final hardening of the material.

Mechanical "cold" processes present several advantages with respect to the thermal and chemical treatments especially in terms of better control of the whole process, reproducibility and interchangeability of parts, and for these reasons are usually preferred.

A lot of surface treatments are industrially used for strengthening metallic components, among them shot peening (SP) is probably the oldest and most famous process used. Other younger technologies like laser shock peening, flap peening, ultra sonic peening and low plasticity burnishing are however considered most effective in imparting residual stresses, despite their more complex set up and higher operational costs.

Laser shock peening is, in particular, object of this work and will be discussed in detail in next chapter with additional comparison with traditional shot peening.

1.4 Bibliography - Chapter 1

[1] H.J. Schmidt. "Damage tolerance technology for current and future aircraft structure".(2005). Plantema Memorial Lecture presented to the 23rd ICAF Symposium, Hamburg, Germany, June 2005

[2] E. Troiani, I. Meneghin, G. Molinari. "Damage Tolerance of Aeronautical Structures". (2010). Lectures of MSc course, II Faculty of Engineering, University of Bologna.

[3] X.Zhang. "Introduction to fatigue analysis".(2008). Lecture notes. School of Engineering, Cranfield University.

[4] W. Schütz. "A history of fatigue". (1996).Engineering Fracture Mechanics 54: 263-300

[5] J. Schijve. "Fatigue of Structures and Materials". (2009). Springer ed.,

[6] P.J. Withers, H.K.D.H. Bhadeshia. "Residual stress Part 1 – Measurement techniques". (2001). Materials Science and Technology April 2001 Vol. 17

[7] P.J. Withers, H.K.D.H. Bhadeshia. " Residual stress Part 2 – Nature and origins". (2001). Materials Science and Technology April 2001 Vol. 17

[8] Macherauch E, Kloss KH. "Origin Measurements and Evaluation of Residual Stress". (1986). Presented at The 1st International conference on residual stresses, Garmisch-Partenkirchen, Germany

[9] D. Broek. "The practical use of fracture mechanics".(1989). Springer Ed.

[10] G.E. Dieter. "Engineering Design". (1986). McGraw-Hill Ed.

[11] S.Y. Oakley, D. Nowell. "Prediction of the combined high and low-cycle fatigue performance of gas turbine blades after foreign object damage".(2007). International Journal of Fatigue, 2007, 29(1): 69–80.

Chapter 2

2. Laser shock peening overview

In order to slow down the manifestation of fatigue related problems in an aircraft, or in any other metallic structure, inserting compressive residual stresses in the zone of interest is one of the problem solving approaches. Among the processes that introduce compressive residual stresses in metallic structures, Laser Shock Peening is an emerging and a promising technique for contrasting the fatigue related phenomena.
In this chapter will be presented an overview of the process and a comparison with an older technology like Shot Peening (SP).

2.1 Fundamentals of LSP

Laser shock peening (LSP) process uses high intensity, short duration laser pulses to induce high shock pressure as an input loading for metallic component processing.
After more than 40 years of research and development, the LSP process has become commercially available and is proposed as a competitive alternative surface enhancement process to improve fatigue resistance of metallic components by generating compressive residual stress.

2.1.1 LSP process

As already mentioned, LSP originates from the ability to drive a high amplitude shock wave into a material surface with a short-pulsed laser with power density of several GW/cm^2 for 1-50 ns.
Fig. 2-1 shows a typical application of this process (in particular the one used by Metal Improvement Company [1]) carried out under confined regime configuration.
A detailed overview of the physics of the process can be found in [2].
The metallic surface is first locally coated with an opaque layer and then is covered by a transparent overlay, such as water.

The opaque coating acts as a sacrificial material to prevent the thermal effect from heating the surface by laser irradiation. A thin layer of it vaporizes upon the absorption of laser energy to generate plasma and for this reason is commonly called *ablative layer*.

The transparent overlay confines the thermally expanding vapor and plasma against the target surface; thus a higher amplitude transient pressure is generated, exceeding the yield strength of the material.

The high shock pressure causes the target to undergo high strain rate deformation (up to 10^6 s^{-1}) during a short time and causes the material to dynamically yield.

If the component to be treated is thick enough or the bottom-side movement is restricted during shock loading, a plastic deformation is mainly generated on top surface and compressive residual stresses are induced to improve the fatigue performance.

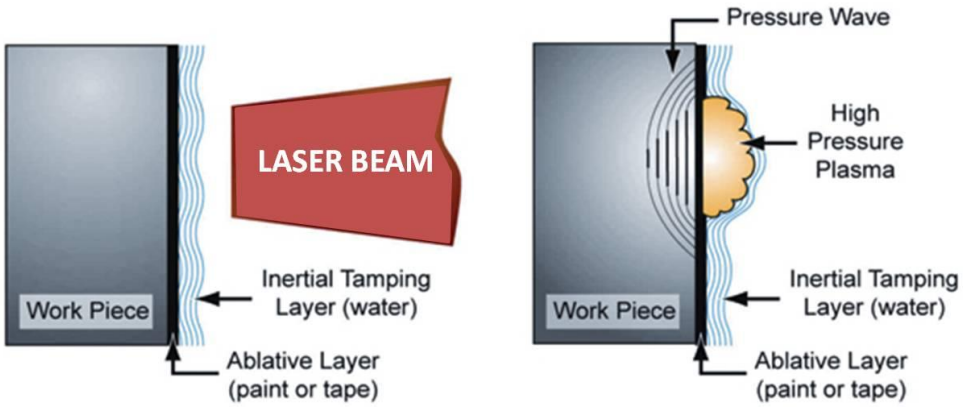

Figure 2-1 Schematic LSP Process [1]

LSP systems for field operations exist, as well, where no ablative layer is used during the exposure to laser pulses, where the treated specimen is emerged into water. This application of LSP, developed by Toshiba, is called Laser Peening without Coating (LPwC) [3].

Since the ablative layer has the function of protecting the surface of the treated specimen from the direct exposition to the high temperature plasma, it's obvious that in absence of it, other precautions must be taken.

Hence the major difference between LSP and LPwC lies in the fact that when no coating is used, the only way to avoid large surface damage is to use lower laser powers combined with very small impact size and high density of impacts, increasing the overlapping of the laser peen spots.

Fig.2- 2 shows a schematic comparison between LSP and LPwC. [4]

The principle of both processes is however the same.

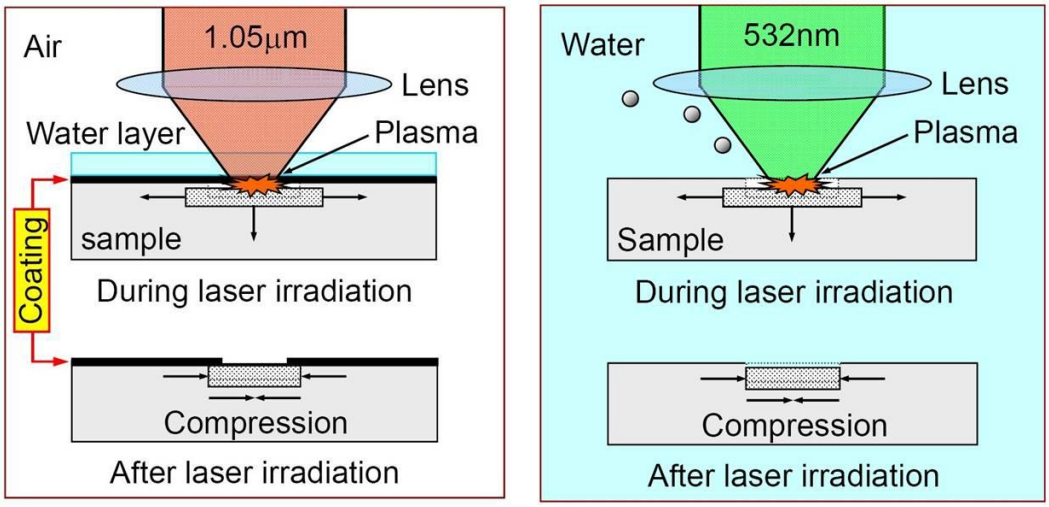

(a) LSP **(b) LPwC**

Figure 2-2 Comparison between LSP and LPwC [4]

2.1.2 Industrial Applications

Laser Peening has been used for several years to prolong the fatigue life of critical aerospace components such as turbine engines and aircraft structures.

Nowadays, the aerospace industry applies LSP to many aerospace products, such as turbine blades and rotor components [5], discs, gear shafts [6] and bearing components [7]. LSP could also be used to treat fastener holes in aircraft skins and to refurbish fastener holes in old aircraft in which cracks, not discernible by inspection, have initiated.

Remarkable improvement to high cycle fatigue performance have been also proved in preventing foreign object damage (FOD) of the turbine engine blades.

Fig.2- 3 shows a Metal Improvement application of LSP on engine blades.

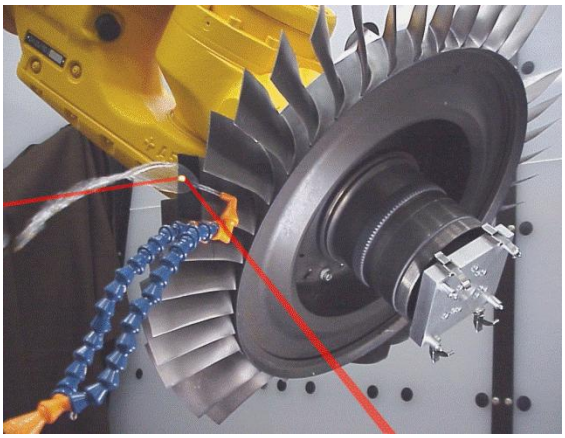

Figure 2-3 MIC application of LSP on engine blades

FOD is most acute on thin edges of titanium airfoils in forward engine stages and left undetected or uncorrected, can dramatically reduce airfoil HCF capability.

FOD or other “naturally” initiated airfoil fractures result in significant secondary damage and generally an in-flight shutdown of the engine being typically a leading cause of unscheduled engine removals.

Since FOD mitigation can have a substantial effect on maintenance costs,in1997 General Electric (GE) Aircraft Engines investigated laser peening as a potential solution to increase the durability of titanium fan blades and decrease their sensitivity to FOD. [8]

Subsequently LSP has been applied in 2002 Rolls-Royce Trent 800 1st fan blade attachment and in March 2003, production of laser peening also commenced on an integrally bladed rotors for Pratt & Whitney's F119-PW-100 engine, used on the F/A-22 Raptor. [8]

Opportunities also exist to apply laser peening for weight reduction, increased reliability, and improved fuel economy in automotive and truck parts such as transmission gears and axles, rotating engine parts, and impellers. Furthermore Medical Applications for Laser Peening include treatment of orthopedic implants to improve the fatigue performance of hip and knee replacement joints and spinal fixation devices. [9]

In last years LSP has been also proved to be effective in forming metallic sheets such as wing skins.

Laser peen forming essentially performs the same role as Shot Peen Forming, but because of the greater depth of plastic work, extends the degree of curvatures possible enabling more fuel efficient profiles to be achieved. [1]

2.2 Comparison with Shot Peening

Shot Peening (SP) is a mechanical surface enhancement technique close to LSP in process and effects. It is a cold working process in which the surface of a part is bombarded with millions of small spherical media, called "shot", which are made of steel, glass or ceramic. In Fig.2-4 it can be seen that each piece of shot striking the material imparts a small dimple to the surface. In order for the dimple to be created, the surface fibers of the material must be yielded in tension [10]. Below the surface, the fibers try to restore the surface to its original shape, thereby producing below the dimple, a hemisphere of cold-worked material highly stressed in compression, as in the case of Laser Shock Peening.

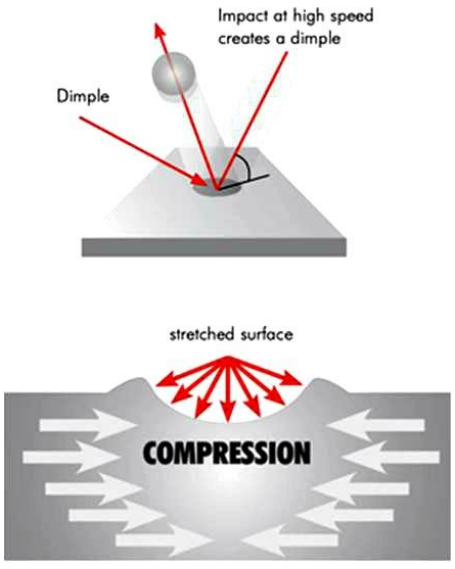

Figure 2-4 Shot peening process scheme [1]

Using SP has several advantages, mostly related to the vast knowledge of the technology.

SP is a relatively simple and inexpensive method to achieve good results in terms of life enhancement, it is also quite flexible since the equipment needed for its application are quite handy and it is possible to use it on large or small areas as required.

These advantages, however, are paid with considerable disadvantages in terms of final results.

First of all the use of small balls makes the process a discrete phenomenon that cannot therefore guarantee a uniform intensity across the component surface. It must be also considered that the balls, once shot, inevitably will contaminated the environment and this is not always allowable.

Lots of investigation has been done on comparison of residual stress induced by SP and LSP and it has been demonstrated that SP has much lower capability .

Fig.2-5 shows the results of a tests campaign done in Ottobrunn by EADS-IW about residual stresses induced by SP and LSP in AA-7050 coupons. Measurements have been done using X-ray diffraction (XRD) and incremental central hole drilling (IHCD) methods.

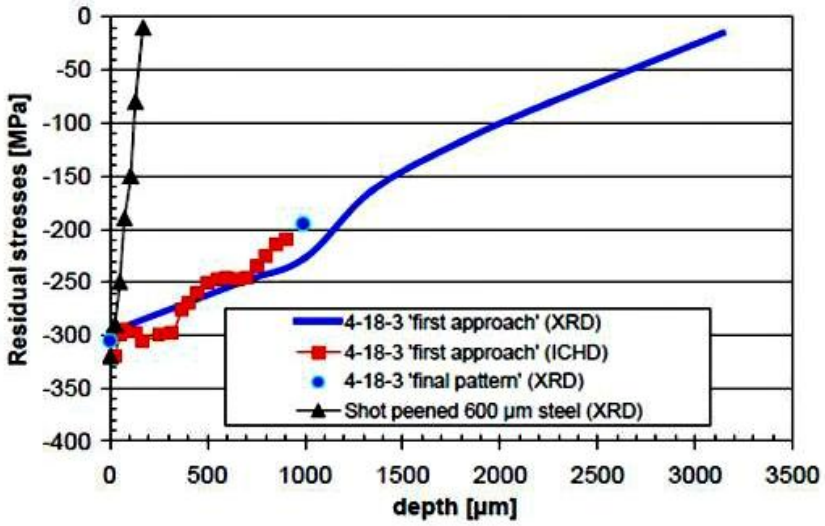

Figure 2-5 Induced residual stress comparison between SP and LSP [11]

As evident SP is very limited in reaching deep compressive stress, while LSP can affect depths from 5 to 10 times larger than SP.

In [11] is also available an investigation on the roughness induced respectively by the two technologies.

Fig.2-6 shows that SP process results in a more roughened surface than the laser peened one. This roughness may need to be removed for some applications, though typical removal processes often eliminate the majority of the peened layer.

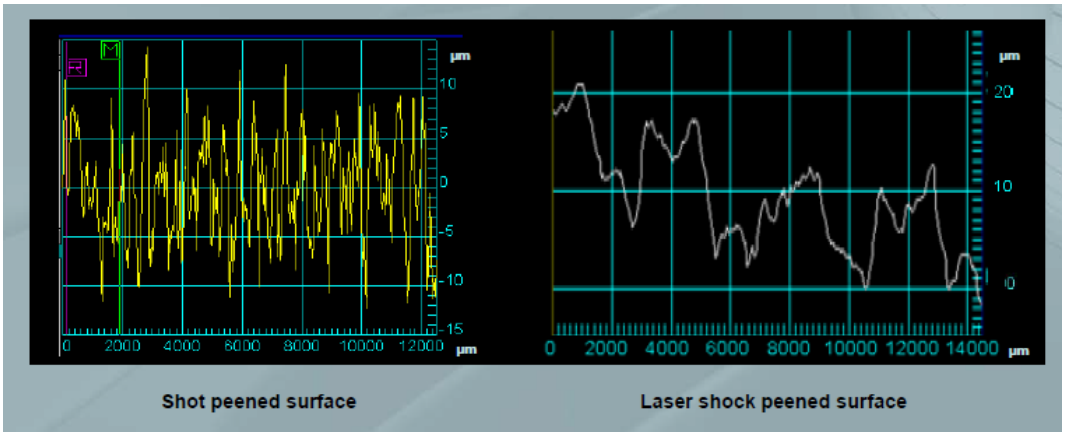

Figure 2-6 Surface roughness profiles for Sp and LSP in [µm] [11]

Investigations on impact of residual stresses on crack initiation and crack growth have also been carried out by EADS-IW and results are shown in Fig.2-7.

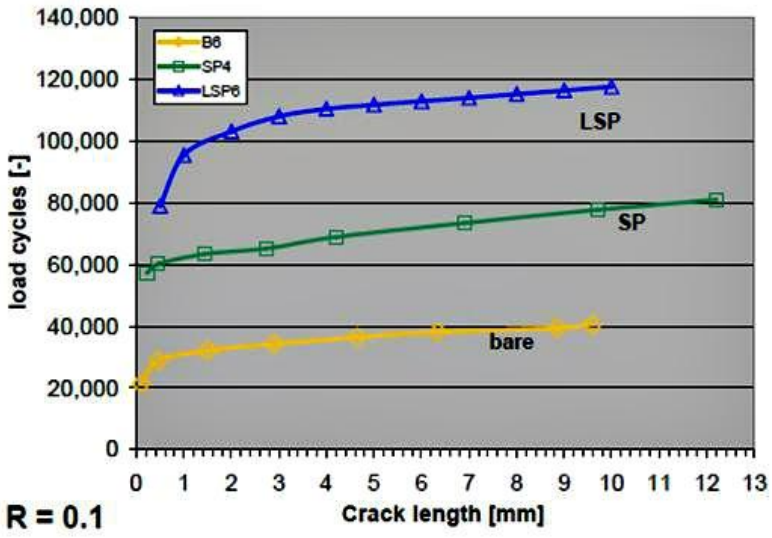

Figure 2-7 Fracture analysis; Comparison between bare, shot peened and laser shock peened [1]

Even in this case an appreciable benefit in terms of fatigue behavior is obtained after the application of both the surface treatments. In particular once again LSP is demonstrated to be more effective than SP with a delayed crack nucleation and a retarded crack growth up to a crack length of ca. 4 mm.

All these considerations rising from experimental results make LSP process definitely more effective of the SP in fatigue life enhancement of the treated component, as shown in Fig.2-8.

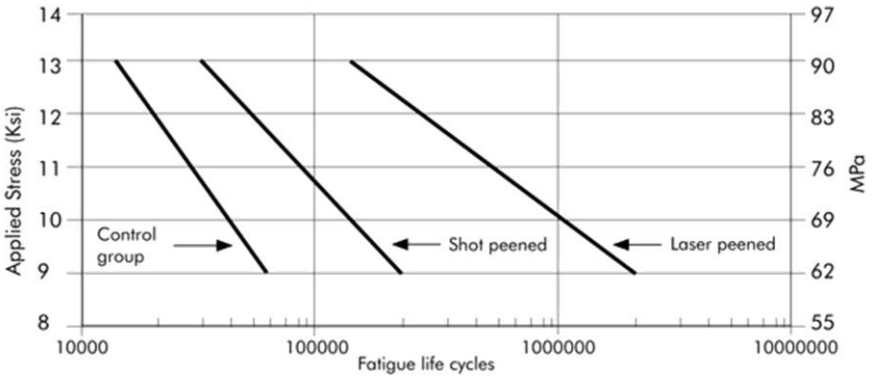

Figure 2-8 Fatigue life comparison between LSP and SP [1]

From the analysis above exposed it is possible to say that LSP cannot be considered as a replacement for conventional SP, but it has additional advantages that makes him unique in surface treatments.

The laser pulse, in fact, can be adjusted and optimized in real time and the spot geometry of laser beam can be changed to suit the problem reaching a control of the process not allowed in SP.

LSP is moreover a "clean" technology that, with the aid of mobile facilities and the newest optical fiber set-up, is able to treat even critical areas.

2.3 Bibliography - Chapter 2

[1] *www.metalimprovement.co.uk*

[2] F.Peyre, R.Fabbro. "Laser shock process: a review of the physics and applications". (1995). Optical and Quantum Electronics 27 (12), 1213–1229.

[3] Y. Sano, N. Mukai, K. Okazaki, M. Obata. "Residual stress improvement
in metal surface by underwater laser irradiation". (1997). Nucl. Instrum. Methods
Phys. Res. B121 (1997) 432-436.

[4] G.Ivetic. " Residual Stress Effects on Fatigue Phenomena in Aerospace Structures". (2010). PhD Thesis in Aerospace Engineering, Faculty of Engineering, Department of Aerospace Engineering, University of Pisa, Italy.

[5] Mannava et al., 5492447, Feb 1996, 415/200; U.S. Patent Documents

[6] Ferrigno et al, 5735044, Apr 1998, 29/889; U.S. Patent Documents

[7] Casarcia et al, 5584586, Dec 1996, 384/625; U.S. Patent Documents

[8] B.Cowles, B.Morris, R.Naik, D.Murphy. "Applications, Benefits, and Challenges of Advanced Surface treatments - An Industry Perspective". (2008). First International Conference on Laser Peening -Houston, Texas
Surface treatments - An Industry Perspective

[9] *http://www.lsptechnologies.com/*

[10] A. Tolga Bozdana. "On the mechanical surface enhancement techniques in aerospace industry – a review of technology".(2005). Aircraft Engineering and Aerospace Technology, Vol. 77 Iss: 4, pp.279 - 292

[11] U. C. Heckenberger, E. Hombergsmeier, W.v. Bestenbostel, V. Holzinger. "LSP to improve the fatigue resistance of highly stressed AA7050 components". (2010). 2nd International Conference on Laser Peening, San Francisco

[12] P.S. Prevéy, J.Cammett. "Low cost corrosion mitigation and improved fatigue performance of low plasticity burnished 7075-T6".

Chapter 3

3 LSP Modeling

3.1 Importance and Application

Since LSP is a relatively young technology, most investigations have been concentrated on experimentally determining its mechanical effects.

All the efforts have been made in order to find out the optimized combination of industrial metals and LSP configuration that realize the best residual stress field and the best surface morphology.

Besides the expense tightly related with the technology application, must be considered all the expenses due to the quite sophisticated measurements techniques like X-Ray Diffraction, Neutron Diffraction, Synchrotron Diffraction, stress contour method, hole drilling and others.

Moreover, the transient nature of the LSP phenomenon makes real time in-situ measurement of laser/material interaction very challenging.

For all these reasons reliable analytical methods for predicting detailed effects of LSP are needed to understand the potential of the process.

Modelling could significantly reduce the development time for new laser peening applications as most of the iterations could be done computationally. From a design perspective, an ideal model of the laser peening process would be one that could accurately predict the total residual stress in an arbitrary three-dimensional body treated with an arbitrary laser peening treatment parameter set, which would allow predicted residual stresses to be used to predict performance improvement. It would be additionally useful if the model could enable optimization of treatment parameters (e.g. irradiance, pulse duration, number of layers, and coverage area).

Finite Element Method was first introduced in 1999 by Braisted and Brockman [1] to investigate the mechanical behavior and predict the residual stresses from the laser shocked materials with software ABAQUS.

From then on several researchers have used ABAQUS to analyze the laser generated shock waves propagating into different materials but the complexity of the LSP process and the big numbers of variables involved in it make hard an intensive development of this studies.

Typical applications of LSP prediction are all the investigations related with the influence on residual stresses and fatigue life of each of the already mentioned parameters like:

- Laser setting parameters (Density of energy, pulse duration, number of layers)
- Geometry of the target (thickness, shape, critical points like edges)
- Laser peening sequence
- Environmental conditions (ablative layer, tamping coat)

Moreover the spreading of LSP in application secondly related to residual compression introduction, put simulations in a strategic position for finding out more and more capabilities of this technology.

It is possible to consider as examples the FEM rule in laser forming process.

A priori information about intensity and distribution of the residual stresses field is, in fact, absolutely necessary for the application of this technology.

Hence, a detailed model able to predict where

3.2 Existing Simulation Methods

As already mentioned, relatively little efforts has been spent in the development of analytical techniques to predict the residual stresses from LSP.

A fundamental reason for the referred lack of predictive capability of LSP processes is their inherent physical complexity, specially due to the coexistence of different material phases (including plasma) developing and interacting under the action of the high intensity laser beam.

However in last ten years lots of trials and improvements of the numerical modeling have been done by researchers.

3.2.1 Explicit/Implicit LSP Analysis Procedure

Some publications [2-4] based on elastic-perfectly plastic solutions assuming uniaxial strain conditions were already available, but the first step towards a more realistic 3D simulation and ad result towards a more accurate prediction has been done by Brockman and Braisted [1].

They used the commercial finite element code ABAQUS to determine both the short duration shock wave response and the resulting residual stress state in the target with the procedure depicted in Fig.3-1.

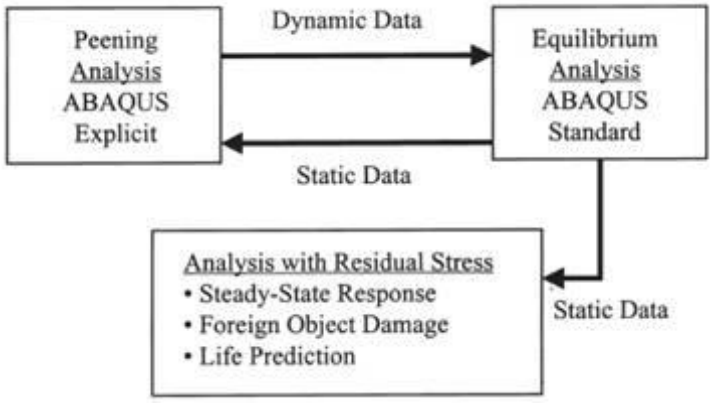

Figure 3-1 Braisted and Brockman [1] LSP analysis procedure

ABAQUS/Explicit is a nonlinear explicit time integration finite element code specifically designed for short duration transient analysis. [15]

ABAQUS/Standard is a nonlinear implicit time integration finite element code used primarily for static or natural frequency calculations. [16]

So the idea of Braisted and Brockman, confirmed by Ding and Ye in 2006 [5] was to perform an ABAQUS/Explicit until all the plastic deformation has occurred.

This running time is typical 2order of magnitude longer than the duration of LSP laser pulse duration to insure all the plasticity has occurred.

At this point the solution is stopped and a restart file containing all the stress, strain and displacement data is generated. This transient stress state is read from the restart file into ABAQUS/Standard to determine the residual stress field in static equilibrium.

To simulate multiple peenings, a restart file from ABAQUS/Standard can be read into ABAQUS/Explicit and the procedure repeated.

A similar strategy has been used by Hu and Yao in 2006 [5] but with different softwares: Ansys and LS-Dyna.

Even in this case FEM analysis procedure of laser shock processing should be composed of two distinct parts including dynamic analysis and static analysis to obtain an absolutely stable residual stress field and surface deformation.

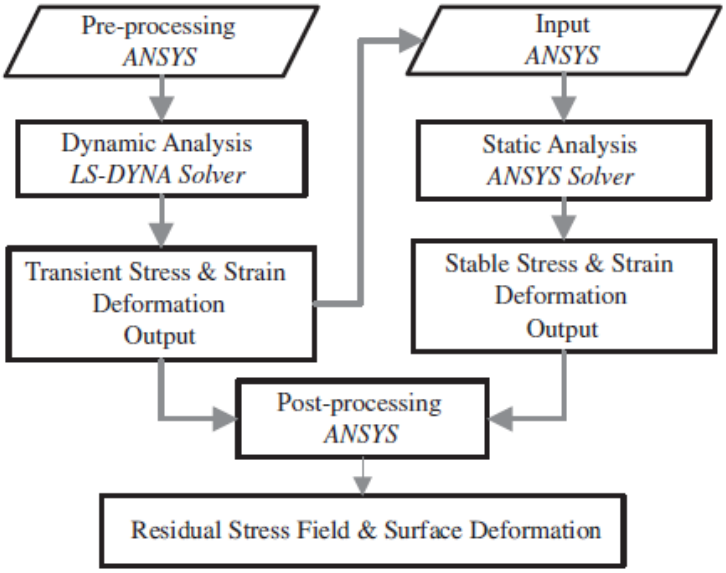

Figure 3-2 - Hu et al. [6] LSP analysis procedure

As highlighted by Fig.3-2 the basic concept is the same of the one proposed by Braisted and Brockman: dynamic analysis is adopted to simulate the propagation of the shock wave and obtain the dynamic response of the material. When the dynamic stress state of the target material become approximately stable all transient stress will be imported into implicit FEM codes to perform static analysis to obtain the residual stress field and the spring-back deformation in static equilibrium.

This is reasonable because explicit methods are well known as the most suitable solver for short time, high speed non linearity problems but they have a lot of convergence issues.

On the other hand implicit methods are more robust and reliable but in solving dynamic problems they have prohibitive computational expenses.

Even if the purpose of using both Implicit and Explicit method is to take advantage of the best features of each code, this analysis procedure seems to be limitative compared with LSP capabilities.
The real issue of this method is, in fact, its poor flexibility.
The FE models described above provide useful insight into the LSP process. However, they are limited to the specific parameters chosen in each case ,and prediction of residual stress state for a different set of laser parameters or a different workpiece geometry requires a new and complex explicit/implicit finite element analysis.

3.2.2 Eigenstrain Method

The needing of a more physically based model which represents the plastic strain introduced by the process, rather than seeking the residual stress field directly, has led researchers to develop the Eigenstrain Method.
The term *eigenstrain*, noted by ε^*, was first suggested by Mr. T. Mura [7] in 1982 to indicate any strain arising in material due to inelastic processes such as plastic deformation, crystallographic transformation or thermal-expansion mismatch between components of an assembly. Eigenstrain accounts for all permanent strains that arise in material exhibiting inhelastic behavior.
In the same period Ueda et. al [8] developed the first method for measuring residual stresses using eigenstrain.
Later, other researchers as M.Hill [9] and Korsunski [10], created more detailed methods based on eigenstrain theory.
Eigenstrain method concept is to model the LSP pulse as a dynamic pressure load in an explicit FE model in order to determine the stabilized plastic strain distribution. This can be then incorporated into a static FE model as an initial misfit strain.
The elastic response of the static FE model will give the residual stress distribution generated by the original shock wave.
The step by step implementation of eigenstrain technique is shown in Fig.3-3.

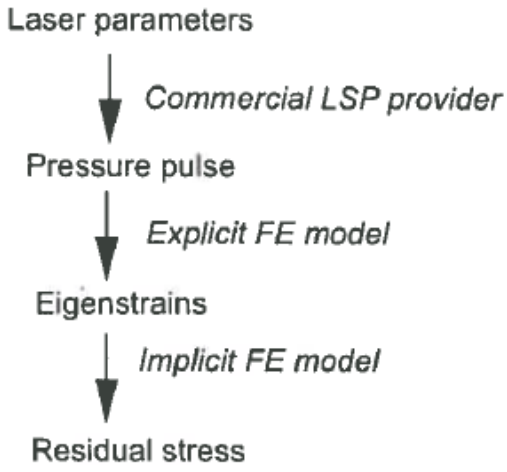

Figure 3-3 - Eigenstrain modelling procedure [11]

At first sight the procedure could seem the same of the one illustrated in in §3.2.1 but the strong point of the method is that once that eigenstrains have been determined, the complete residual stress distribution can be reconstructed through a single elastic analysis.

Another big advantage of this technique is that the stabilized plastic strains generated by LSP depend on the parameters of the laser pulse but are largely independent of the specimen geometry.

In this way once the eigenstrain distribution caused by a particular laser pulse has been determined, it can be used to evaluate the residual stresses caused by the same pulse in a range of other geometries.

To better understand how this method works we can consider the additive decomposition of total strain to be expressed via the sum of elastic strain and eigenstrain:

$$\varepsilon = \varepsilon_e + \varepsilon^* \tag{3.1}$$

where ε_e is the elastic strain and ε^* is the eigenstrain and small strain approximation is adopted.

Moreover we can consider $\varepsilon^* = \varepsilon_{pl} + \varepsilon_{th}$ i.e. the sum of the plastic strain and the thermal strain. When an eigenstrain ε^* is prescribed in a finite local domain in an homogeneous elastic material, the incompatibility of displacement would generate residual stress and distortion with the total strain.

Since in the LSP process both the laser-ablation-induced heating and the shock-induced thermal effect can be neglected we can simply assume that eigenstrain is only represented by the plastic deformation.

After the plastic strain is generated by the shock, the plastically deformed material stays in geometric compatibility with the remaining material and the residual stress state develops as the remaining material pushes the plastically deformed materialback towards its original position into a configuration that satisfies both the deformation compatibility and the stress equilibrium. Therefore, the residual stress and deformation fields for different LSP processes can be solved as an elastic problem based on the determined eigenstrain embedded in the model, without concern for the complex dynamic response of the material.

It is clear that a so simple method cannot catch the whole dynamic response of the process so it cannot take into account all the effects related with the presence of edges or the reflection of the stress waves from the boundary conditions and it is also confined to the small strain condition.

Hence, it is possible to say that eigenstrain method is really effective in determination of "hot spot" that is area affected by compressive rather than tensile stresses.

Nevertheless the reliability and flexibility of this technique are counterbalanced by the scarce accuracy in material behavior modeling.

Eigenstrain method doesn't take into account all the phenomena caused by "special" geometries of the targets, it has also several issues in prediction of residual stresses in thin part that could feel the influence of the geometrical boundary conditions.

3.2.3 ShockLas Prediction Tool

The above-mentioned methods try to induce the intensity and temporal profile of the shock wave without any reference to the detailed physics of the plasma formation process taking place in the outermost layers of the solid target: this plasma is assumed to be built up to certain degree as a consequence of the initial laser energy deposition, but no analysis is provided about its real dynamics.

In 2004 Ocaña et.al.[12] presented a theoretical and computational method called Shocklas for the analysis and predictive assessment of LSP processes. Shocklas has been developed in order to simulate each phase of the LSP in a self-consistent way from the physical point of view.

The referred phase are the following :

- Analysis of the plasma dynamics, including consideration of breakdown phenomenology in the dielectric media.
- Simulation of the hydrodynamic phenomenology arising from plasma expansion between the confinement layer and the base material.
- Analysis of the propagation and induction of permanent structural changes by shock wave evolution in bulk material.

The calculation model, Shocklas, integrates all those three phases respectively in three modules called *HELIOS*, *LSPSIM* and *HARDSHOCK*.

In Fig.3-4 a schematic representation is shown on the way of coupling of the referred modules.

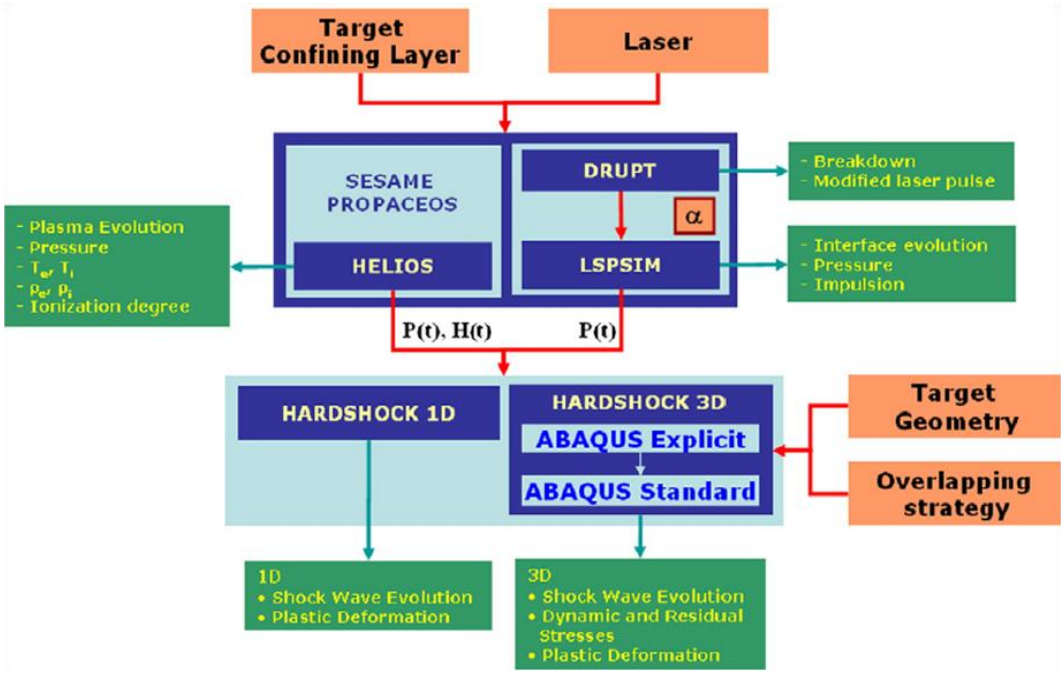

Figure 3-4 Shocklas calculation scheme [13]

HELIOS is a 1-D radiation-magnetohydrodynamics code that is used to simulate the dynamic evolution of laser created plasma.

LSPSIM is a 1-D model intended for the estimation of the pressure wave applied to the target material in laser shock experiments [12,14].

It provides a direct input interface for the detailed plasma results obtained by *HELIOS* for the first short times of the laser interaction, and, second, it provides a time dependent estimate of the pressure build-up and mechanical target compression in longer times when the generated plasma has been exhausted and the shocking dynamics is dominated by gas expansion. More concretely, *LSPSIM* analyzes the material tamper gap assuming a only phase of evolution that can be extended to the end of the processes, i.e. obtains the target-confining medium gap amplitude, by solving the coupled system of energy and impulse equations subject to the thermofluid-dynamic conditions imposed by the laser energy deposition.

HARDSHOCK solves the shock propagation problem into the solid material on the basis of the time-dependent pressure profile calculated by *HELIOS* or *LSPSIM*.

It has a specific consideration of the material response to thermal and mechanical alterations induced by the propagating wave itself. (i.e. affects as elastic-plastic behavior. changing in elastic constants, phase changes etc..)

The 3-D version of the code has been developed on the base of FEM commercial code ABAQUS using an explicit differencing strategy for the initial fast shock propagation and a standard implicit differencing strategy for the analysis of the final residual stresses equilibrium.

Hence, it is possible to conclude that Shocklas is a powerful calculation method that allows a systematic study of LSP processes starting from laser-plasma interaction.

The integrated laser-plasma analysis routine, based in realistic material EOSs, provides a unique capability for process parameterization.

Additionally, the development of the appropriate experimental diagnosis facilities and the connection of numerical simulation to experimental material characterization results enable a fundamental and reliable process understanding capability in view of process industrial implementation.

A so accurate simulation, however, is paid by huge computational costs.
At a researching level these costs can be accepted, but thinking in an industrial point of view is quite unreasonable to take into account so long time for simulations.

3.3 New Simulation Approach

Aim of this work is therefore to find a simulation method that could be placed half-way between eigenstrain method and Shocklas calculation tool.
In other words, the objective is to realize a tool which includes the following characteristics:
User Friendly. In this purpose it has been decide to develop a method based on the commercial code ABAQUS that is widespread in the most part of industrial companies.
Reliability. An intensive campaign of experimental tests has been done to guarantee the possibility to calibrate the model and to verify the reliability in different peening conditions and for different target geometries.
Modeling-Time Optimized. The method has been developed using only the Explicit/ABAQUS code in order to allow the user to run the analysis in only one step.
The Explicit code will, at the same time, guarantee the convergence even for the first "fast impact" phase.
All the details of the method will be described punctually in the following Chapters §4 and §5.

3.4 Bibliography - Chapter 3

[1] W. Braisted, R. Brockman."Finite element simulation of laser shock peening". (1999). International Journal of Fatigue 21 (1999) 719-724.

[2] P.Peyre, R.Fabbro, L.Berthe, C.Dubouchet. "Laser shock processing of materials." (1996). J Laser Appl; 8:135-41

[3] P.Peyre, R.Fabbro, P.Merrien, H.Lieurade. "Laser shock processing of aluminum alloys. Application to high cycle fatigue behavior." (1996). Mater Sci Engng; A210:1996.

[4] P.Ballard. "Residual stresses induced by rapid impact-applications of laser shocking." (1991). Ecole Polytechnique.

[5] K.Ding, L.Ye. "Laser shock peening: performance and process simulations. (2006). Woodhead, Cambridge, UK.

[6] Y.Hu, Z.Yao, J.Hu. "3-D FEM simulation of laser shock processing." (2006). Surf. Coat. Technology; 201(3/4),1426-1435.

[7] T.Mura. "Micromechanics of defects in solids". (1982).Martinus Nijhoff Publishers, Dordrecht.

[8] Y.Ueda, K.Fukuda, Y.C.Kim. "New measuring method of axysimmetric three-dimensional residual stresses using inherent strains as parameters." (1986). J. Engng Mater. Technol. 108(4), 328-334.

[9] T.L.Panontin, M.R.Hill. "The effect of residual stresses on brittle and ductile fracture initiation predicted by micromechanical models." (1996). Int. J. Fract. 82(4), 317-333.

[10] A.M.Korsunsky. "Residual elastic strain due to laser shock peening: modelling by eigenstrain distribution." (2005). J. Strain Analysis 41(3),195-204.

[11] M.Achinta, D.Nowell."Eigenstrain modelling of residual stresses generated by laser shock peening". (2011). J. Mater. Porcess. Technology 211(2011),1091-1101.

[12] J.L.Ocaña, M.Morales, C.Molpeceres, J.Torres. "Numerical simulation of surface deformation and residual stresses fields in laser shock processing experiments." (2004). Appl. Surf. Sci. 238(2004), 242-248.

[13] M.Morales, J.L.Ocaña, C.Molpeceres, J.A.Porro, A.García-Beltrán. "Model based optimization criteria for the generation of deep compressive residual stress fields in high elastic limit metallic alloys by ns-laser shock processing." (2008). Surface&Coatigs Technology 202(2008),2257-2262.

[14] J.L.Ocaña, C.Molpeceres, M.Morales, A.Gracìa-Beltràn. C.R. Phipps, M. Niino (Eds.), High-Power Laser Ablation II SPIE Proceedings,3885, 2000, p. 252.

[15] Dassault Sistèmes. "Explicit Dynamic analysis". Abaqus Theory Manual. (2011). §2.4.5

[16] Dassault Sistèmes. "Implicit Dynamic analysis". Abaqus Theory Manual. (2011). §2.4.1

Chapter 4

4 FE Explicit Analysis Methodology

In this Chapter will be provided a detailed description of all the parameters that Abaqus Explicit needs to perform a correct simulation of LSP process.
It will also analyze the characteristic values used in another work that will be the starting point for the optimization of the whole simulation.

4.1 Everything ABAQUS/Explicit needs to perform a simulation

The ideal model for LSP needs to incorporate the laser beam parameters, overlay conditions and material properties, to enable the final outcome of the process in terms of processing conditions to be specified. [1]
This paragraph will present an overview of the most important processing phases required for an ABAQUS/Explicit analysis. [11]

4.1.1 3-D Model and Mesh

The ABAQUS commercial software packet include a CAE tool with which is really easy to create a 3-D model [9].
The interface is similar to every other computer assisted design software: you can start with a 2-D sketch and then perform all the actions typical of manufacturing processes (i.e. extrusion, fillet, section-cut, etc.).
Once the 3-D overall model has been created it is necessary to define several features that are needed to complete the preprocessing work [10].
Especially in multiple spots and multiple layers analyses is helpful to pre-define the surfaces that identify every laser shot.
(This procedure is also used in the real LSP process to map the peened area).
To do this, several partitions are needed in both surfaces and cells.

Fig.4-1 shows an example of partition and its correspondence with the laser shots.

As the semi-transparent image hihglight, the partition involves not only the surfaces but the whole solid that results divided in cells.

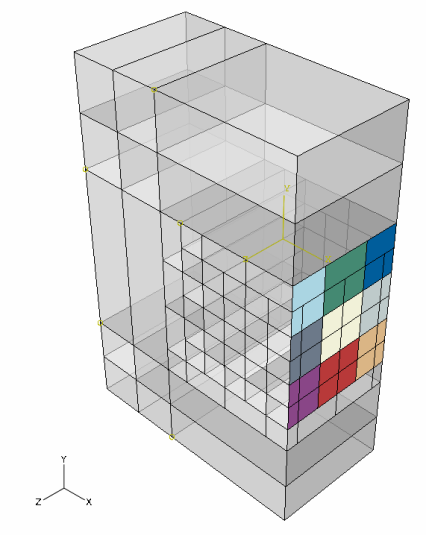

Figure 4-1 Solid partition and laser shots

For this reason particular attention must be paid on doing partitions.

It must, in fact, consider that every partition creates one or more edges. Each edge needs a seed assignment to guarantee a good quality of the mesh. So it is obvious that having a big number of edges means delay the preprocessing time.

In the other hand, not assigning properly the number of seeds produce a uniform elements mesh that is not optimized and that will take longer CPU's time.

(For more details on mesh optimization technique see next chapter) .

4.1.2 Material Equation of State (EOS)

Even though the purpose of this work is not to model all the laser shock peening process phases nor to go through the physics of each of these phases, some theoretical mentions are needed in order to be able to develop a realistic model.

As already mentioned in chapter §2 residual stresses in LSP treated components are induced by a shock wave [2,3].

The shock front experiences an hydrodynamics discontinuity governed by the following equations [4]:

$$\text{Conservation of Mass : } \rho_0 U_s = \rho(U_S - U_P) \tag{4.1}$$

$$\text{Conservation of Momentum : } (P - P_0) = \rho_0 U_S U_P \tag{4.2}$$

$$\text{Conservation of Energy : } (E - E_0) = \frac{1}{2}(P + P_0)(V + V_0) = \Delta E \tag{4.3}$$

Where "*s*" subscript indicates all the quantities related to the shock wave, "*p*" subscript indicates all the quantities related to the particle and the "*0*" refers to quantities for undisturbed conditions.

Observing equations (4.1), (4.2) and (4.3) it is possible to identify five variables (U_S, U_P, E, P, ρ) that makes the system of equations undetermined.

For this reason, at least one more equation is needed to determine all parameters as a function of only one of them. This equation is typically called *equation of state (EOS)* that is strictly related to the characteristics of the process and of the material.

Several type of these equations are available in literature but choosing one of them is not a trivial problem, specially for using in simulation of particular processes like LSP.

It must be taken into account, in fact, that LSP generates strain-rates exceeding $10^6 s^{-1}$ within the target material. At such rates, metals behave significantly differently than under quasi-static conditions. As the strain-rates increases, metals typically exhibit little change in elastic modulus and an increase in Yield strength.

For this reason an accurate material model is needed to simulate the material behavior.

Amarchinta et al. in [5] presented a brief overview of the three most popular formulations.

4.1.2.1 Elastic perfectly plastic (EPP) model

In the EPP model, no strain hardening and/or strain rate dependence is considered. Once the plastic regime is reached, the stress remains constant. The yield stress is derived based on Hugoniot elastic limit (HEL) because LSP is a shock wave phenomenon. HEL is defined as the axial stress required for plastic deformation under uniaxial strain conditions. It is assumed that yielding occurs when the stress in the direction of shock wave reaches the HEL. Where HEL and σ^y are correlated by the following equation:

$$\sigma^y = HEL\ \frac{(1-2\upsilon)}{(1-\upsilon)} \tag{4.4}$$

where υ is Poisson's ratio.

The advantage of this model is that only a small amount of data is required to estimate the yield stress. The disadvantage is that it does not account for strain hardening and/or strain rate dependence.

4.1.2.2 Zerilli-Armstrong (ZA) Model

The ZA constitutive model is based on dislocation mechanics and the crystal structure of the material [6]. There are several generations of the model. Initially, the model addressed face centered cubic (*FCC*) and body centered cubic (*BCC*) structures. The flow stress relationship is shown in equations (4.5) and (4.6) for fcc and bcc structures, respectively:

$$\sigma = C_1 + C_5\varepsilon^n \exp\left(-C_3T + C_4T\ ln\dot{\varepsilon}\right)\ [FCC] \tag{4.5}$$

$$\sigma = C_1 + C_2 \exp(-C_3T + C_4T\ ln\dot{\varepsilon}) + C_5\varepsilon^n\ [BCC] \tag{4.6}$$

C_1, C_2, C_3, C_4, C_5 and n are material constants that need to be determined. C_1, C_5 and n are similar to A, B and n, respectively, of the JC model. The work has been extended to include strain recovery for hexagonal closely packed (hcp) metals [7]. Equation (4.7) shows the constitutive model:

$$\sigma = \sigma_a + Be^{-(\beta_0-\beta_1 \ln \dot{\varepsilon})T} + B_0\sqrt{\varepsilon_r(1-e^{-\varepsilon/\varepsilon_r})}\, e^{-(\alpha_0\alpha_1 \ln \dot{\varepsilon})T} \quad (4.7)$$

where σa, B, β0, β1, B0, εr, α0 and α1 are the constants that need to be estimated. The term in the square root is the strain recovery term. This addresses the shear instability, an important consideration for hcp structures (Ti–6Al–4V). The ZA model considers the interaction effect between strain rate and temperature. The disadvantage of the ZA model is that it has a high number of constants to determine.

4.1.2.3 Johnson-Cook (JC) Model

JC is one of the most frequently used models for impact studies [8]. The JC model describes the flow stress (σ) of the material as a product of three terms: a strain hardening term, a strain rate dependent term and a thermal term as described by (4.8).

$$\sigma = [A + B\varepsilon^n]\left[1 + C \ln\frac{\dot{\varepsilon}}{\dot{\varepsilon_0}}\right][1 - T'^m] \quad (4.8)$$

where :

$T'^m = \frac{T-T_r}{T-T_m}$ with T_r room temperature and T_m melting temperature;

A, B, n, C, $\dot{\varepsilon_0}$ are experimentally determined with split Hopkinson bar tests for strain rates up to $10^4 s^{-1}$.

Parameter A is the initial yield strength at room temperature. Parameter n takes strain hardening into account, while parameter m models the thermal softening. Parameter C represents the strain rate sensitivity.

The main advantage of the JC model is that the estimation of the parameters is simple and easy because it allows isolation of the three effects. This can also be a disadvantage, as it does not take interaction effects into consideration.

For all the considerations exposed above, JC material model has been chosen in this work as the most suitable for the simulation optimization.

4.1.3 Steps and Load definitions

The next preprocessing step needed is to define all the parameters related with laser settings .

4.1.3.1 Pressure Load - Temporal Profile

Plasma conditions are simply modeled as a pressure load. [12]

The pressure load is applied with a realistic temporal profile that corresponds at the temporal profile of the Laser pulse as shown by Fig.4-2.

The plot illustrates the laser and pressure pulses, monitored with a fast photodiode and an x-cut quartz gauge system respectively. It can be observed that the decay time is much slower for the stress pulse than for the laser pulse because of plasma

confining effects. These higher stress wave durations are expected to increase the amount of shock-induced cold work, mainly for low-strength materials such as aluminum alloys.

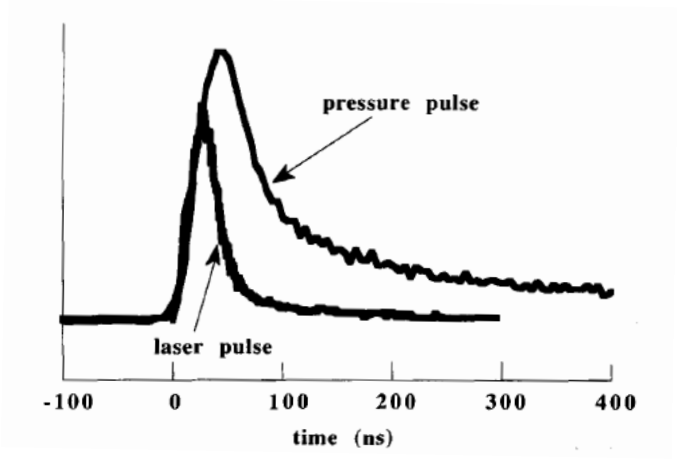

Figure 4-2 Laser Pulse and resulting Pressure load [14]

This profile can be easily modeled in one of the way suggested by Fig.4-3.

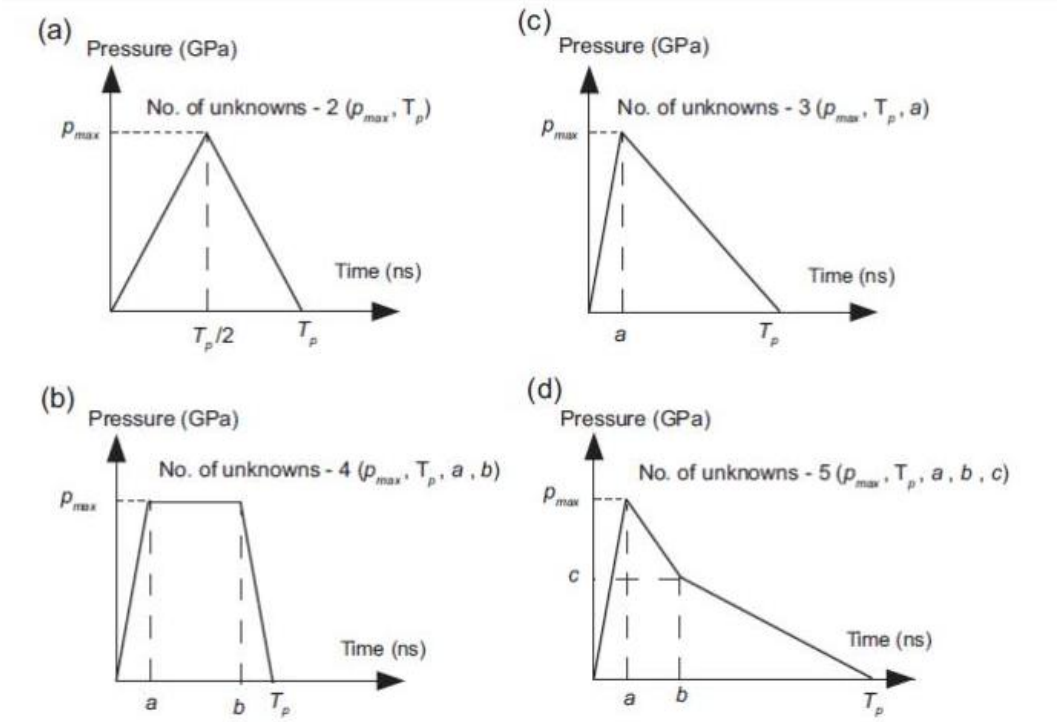

Figure 4-3 Approximations of pressure-time variation [18]

The peak of pressure generated by the laser pulse is dependent by the condition under which the process is realized.

For the confined ablation mode, that is the one treated in this work, a precise description has been given. [17]

Considering the plasma to be a perfect gas, the relationship between the three steps of the pressure generation (heating, adiabatic cooling and final expansion) is given by the following law:

$$P\ (GPa) = \ 0.01 \sqrt{\frac{\alpha}{2\alpha+3}} \sqrt{Z(g\ cm\ s^{-1})} \sqrt{I_0(GW\ cm^{-2})} \qquad (4.9)$$

where I_0 is the incident laser power density, P is the pressure, Z is the reduced shock impedance between the target and the confining medium and α is the efficiency of the interaction.

In a water confinement mode the equation (4.9) gives

$$P\ (GPa) = \ 1.02 \sqrt{I_0(GW\ cm^{-2})} \qquad (4.10)$$

Using (4.10) is therefore possible to easily find a direct correlation between the laser setting and the peak pressure that has to be set in the ABAQUS simulation.

4.1.3.2 Pressure Load - Spatial Profile

As already mentioned in §4.1.1, to simulate the single peen and consequently to apply the correct peening sequence several partitions of the surfaces are needed.

This partitions are useful to apply the pressure load with its related peak of intensity by using a specific Abaqus/Explicit load module, called indeed *pressure.*

In this module must be specified the area of the application of the load and this operation can be easily performed using the partitioned surfaces.

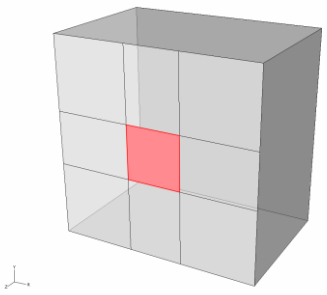

Figure 4-4 Peened Area definition

In Fig.4-4 is possible to see an example of peened area definition highlighted in red.

It must be noticed that in all the works done till now the pressure load defined in the highlighted area is a uniform load equal to the pressure peak value.

The use of this uniform spatial profile is in fact the fastest in terms of preprocessing.

However, investigations done with this work, highlighted some problems of discontinuity at the boundary between the peened and the unpeened area that can be reduced by using a non-uniform spatial profile.

More details about this topic can be found in next chapter §5.

4.1.3.3 Steps

Each pressure load is introduced in a step [13] in which all the numerical settings (i.e. step duration, numerical damping, integration method, output requests) must be set.

The typology of the step set the type of analysis that will be performed.

In our case all the steps are Dynamic, Explicit.

It must be noticed that the step duration and, subsequently, the integration time of the solver must be set in strict relation with the mesh size.

As it will more deeply explain in Appendix A, ABAQUS/Explicit use the central difference scheme that is conditionally stable.

The stability limit can be defined using the element length L^e, and the wave speed of the material C_d:

$$\Delta t = \min\left(\frac{L_e}{C_d}\right) \tag{4.11}$$

where:

$$C_d = \sqrt{\frac{E}{\rho}} \text{ and } L_e \text{ is the length of the mesh element} \tag{4.12}$$

In the step modulus other features like artificial damping (Bulk Viscosity) or mass scaling can be set if needed.

4.2 Previous investigations

The idea to develop this method is not new.

Ivetic [15] and Sticchi [16] already have done several investigations on optimization of the parameters settings and have found out some interesting results.

These works have been used as stepping stone to reach a better understanding of the physical meanings of each parameter.

In particular in [15] the author performed a numerical analysis of LSP process applied to an open hole specimen, representative of a section of an aircraft fuselage lap joint, typically prone to fatigue crack nucleation at the rivet holes. A standard explicit/implicit process has been applied and the results were compared in with different solutions for the insertion of compressive residual stresses around fastener holes in thin-walled structures.

From a strictly numerical point of view, the author focused his attention on finding out which material model could be most adequate to simulate the real material behavior under LSP process condition. The work highlighted the Johnson Cook model as the most appropriate for this kind of analysis.

In [16] this material model is used to realize a first calibration of the model: starting from the real Al7050-T7451 specimen geometry (Fig.4-5), a simulation strategy has been developed (Fig.4-6).

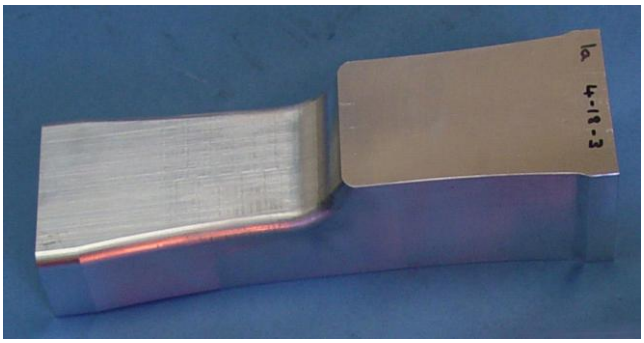

Figure 4-5: Real Specimen Geometry

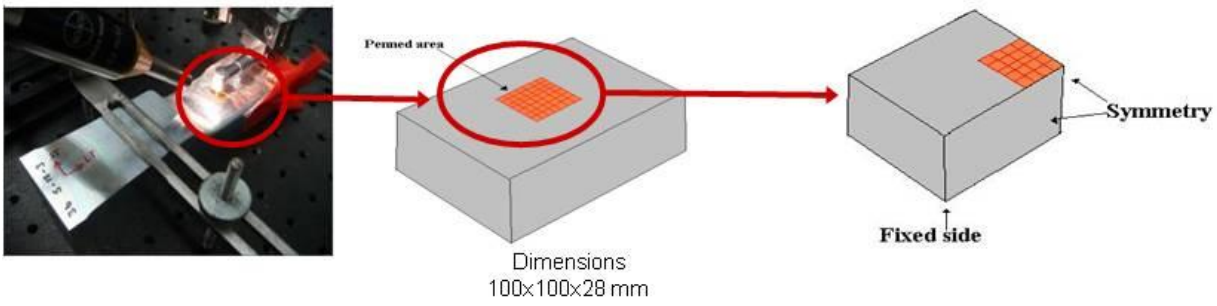

Figure 4-6 Simulation Strategy.

As it can be seen from Fig.4-6, because of the symmetry of the peened block, only one quarter of the piece has been modeled in order to reduce computational costs. The same approach has been used in investigations about geometry effects on residual stresses.

All the investigations done seemed to have a good correlation with the experimental results and enabled the parameters used to be considered reliable.

Tab.4-1 summarizes the settings related with the last simulations and used for starting the new investigation.

<table>
<tr><th>Parameter</th><th>Setting</th><th>Description</th></tr>
<tr><td>Laser Setting</td><td>4-18-2</td><td>The specimens for experimental measurements has been treated with Metal Improvement Laser Facility</td></tr>
<tr><td>Peak Pressure</td><td>3500</td><td>The relation (9) gives a value of the peak pressure a bit greater than 3500MPa, but private discussions with MIC specialists brought authors to round-down that value.</td></tr>
<tr><td>Pressure Temporal Profile</td><td>Triangular</td><td>It has been considered the simplest way to model the temporal profile</td></tr>
<tr><td>Full Width at Half Maximum (FWHM)</td><td>60 ns</td><td>This is the point in the temporal profile in which the peak of pressure is reached. Investigations on the influence of FWHM has been done in [16].</td></tr>
<tr><td>Artificial Damping</td><td>Default</td><td>No investigations on artificial damping influence has been done.</td></tr>
<tr><td>Material Model</td><td>Johnson Cook</td><td>The following parameters has been used for Al 7050-T7451 [19]
<table>
<tr><td>A [MPa]</td><td>B [MPa]</td><td>n</td><td>C</td><td>ε_0</td><td>m</td></tr>
<tr><td>490</td><td>207</td><td>0.344</td><td>0.005</td><td>1</td><td>1.8</td></tr>
</table>
</td></tr>
</table>

Tab. 4-1 Parameters settings for starting point analysis

Once that the settings has been calibrated, the author in [16] carried also out some investigations on geometry dependence of the residual stress.

For this investigations a new specimen has been used and subsequently a new model geometry as well.

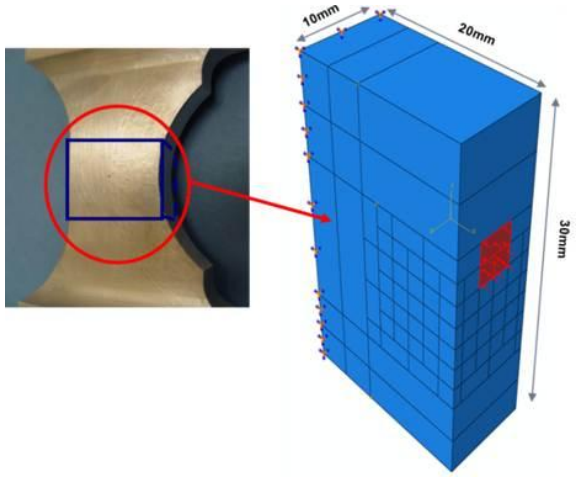

Figure 4-7: Modeling strategy for geometry investigations

It was noticed that approaching the sharp edge, there is a significant drop of the compressive residual stresses.

For that reason it has been investigated the influence of rounding the edges or using a chamfer[16].

4.3 Bibliography - Chapter 4

[1] Y.Hu, Z.Yao. "Numerical simulation and experimentation of overlapping laser shock processing with symmetric cell". (2008). Int. Journal of Machine Tools & Manufacture 48(2008),152-162.

[2] M.A.Meyers,. "Dynamic Behavior of Materials." (1994). J. Wiley, 668 pages, ISBN: 047158262X

[3] Y.M.Gupta. "Shock Waves in Solids".(2001) Course Notes:
Physics 592, Washington St. University.

[4] M.B.Prime. "Everything Engineers need to know to model shock behavior of Metals". (2008). Los Alamos National Laboratory Report LA-UR-08-7939.

[5] H.K. Amarchinta, R.V.Grandhi, K.Langer, D.S.Stargel. "Material model validation for laser shock peening process simulation". (2009). Modelling Simul. Mater. Sci. Eng. 17(2009) 015010 (15pp).

[6] F.J.Zerilli, R.W.Armstrong. "Dislocation-mechanics-based constitutive relations for materials dynamic calculations" (1987) J. Appl. Phys. 61, 1816–25

[7] F.J.Zerilli. "Dislocation mechanics-based constitutive equations Metall". (2004) Mater. Trans. A 35 2547–55

[8] G.R.Johnson, W.H.Cook . "A constitutive model and data for metals subjected to large strains, high strain rate and high temperatures". (1983) Proc. 7th Int. Symp. on Ballistics (The Hague, Netherlands) pp 541–47

[9] Dassault Sistèmes. "Creating and analyzing a model using the Abaqus/CAE modules ". Abaqus/CAE User's Manual. (2011). Part III

[10] Dassault Sistèmes. "Using feature-based modeling effectively ". Abaqus/CAE User's Manual. (2011). §11.10

[11] Dassault Sistèmes. "Explicit Dynamic analysis". Abaqus Theory Manual. (2011). §2.4.5

[12] Dassault Sistèmes. "Load cases". Abaqus/CAE User's Manual. (2011). §34

[13] Dassault Sistèmes. "The step module". Abaqus/CAE User's Manual. (2011). §14

[14] P.Peyre, R.Fabbro, P.Merrien, H.P.Lieurade. "Laser shock processing of aluminium alloys. Application to high cycle fatigue behaviour". (1996). Material Sci.Eng. A210(1996),102-113

[15] G.Ivetic'. "Finite Element Analysis of Laser Shock Peening of Aluminum Alloy 7050-T7451 Thick Plates". (2009). Alma Mater Studiorum University of Bologna.

[16] M.Sticchi. "Finite element modelling of Laser Shock peening-Geometrical Constraints Impact on Residual Stress Distribution After Laser Shock Peening". (2011). University of Neaples "Federico II".

[17] R.Fabbro, J.Fournier, P.Ballard, D.Devaux, J.Virmont. "Physical study of laser produced plasma in confined geometry". (1990). J. Appl. Phys. 68(1990),775

[18] M.Achintha, D.nowell. "Eigenstrain modelling of residual stresses generated by laser shock peening". (2001). J. Mater. Process Tech. 211(2011),1091-1101.

[19] L.Zhanqiang, S.Zhenyu, G. Yuebin: "Fem Simulation of Minimum Uncut Chip Thickness in Mechanical Microcutting". (2006) ISMNM 2010 – Guilin and Han et al., 2006

Chapter 5

5 Optimization and calibration

In this chapter a deep analysis of the optimization strategy for the numerical model will be presented.

Obviously the dissertation will start from the problems noticed in the previous works and it will reach step by step a new optimized simulation strategy that can be considered more reliable and robust.

5.1 Previous investigations problems

The first aim of this work was the wish to complete the previous one done by Sticchi in [1]. It was required to integrate the set of investigations on geometry constrains impact on residual stress distributions after laser shock peening.

In particular simulations on sharp, chamfer and 4 mm round edge models were already available and it was needed to understand which was the radius that minimize the drop of residual stresses approaching the edge.

A first simulation with a 2 mm round edge model was performed. As can be seen in Fig.5-1 (a) the presence of a smaller radius required the use of smaller mesh elements in order to fit the corner as best remembering that the corner was just the critical area in which the investigation was focused. For this reason was absolutely not allowed to use a rough mesh or a discontinuous one.

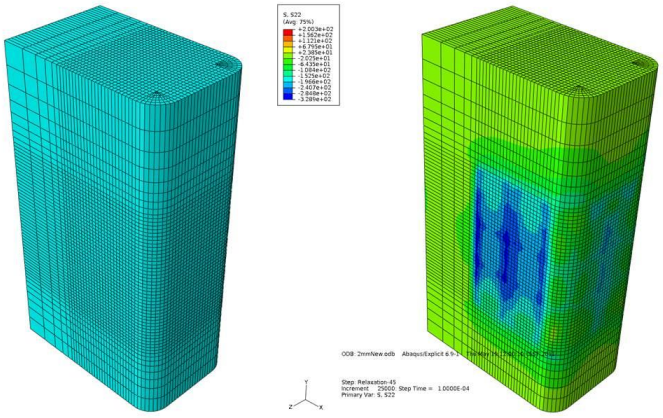

(a) **(b)**

Figure 5-1 Mesh and simulation result for 2 mm radius model

In Fig.5-1 (b), however, it is possible to notice that using so small mesh elements led to resulting stress values that exceeded a lot the expected ones.

This phenomenon has been interpreted as a clear proof of the mesh sensitivity of the model.

Is, in fact, well known that increasing the number of elements and reducing them size means to have a better accuracy of the simulation i.e. to be able to capture more in detail any variations.

In the other hand small mesh elements are more inclined to numerical instability especially in highly dynamic analyses.

Hence it was decided to conduce a mesh sensitivity investigation.

Moreover another point was not clear in the previous study and it concerns the parameters involved in the JC material model.

The ones used in the previous work were found in [2] and has been considered the most suitable because of good correlation between simulations and the experimental results.

The rising up of the mesh sensitivity problem, however, renewed the problem about these parameters that are insufficiently mentioned in literature.

Starting from the above mentioned consideration a new outline of the work has been planned in order to solve all the problems found in the previous investigations and to have a deeper physical insight of all the parameters involved in the simulation.

5.2 Mesh Sensitivity and Optimization

In order to confirm the mesh sensitivity of the simulation and to get started the optimization process a simple analysis has been performed.

Fig.5-2 shows the simple cubic model that has been chosen for this purpose.

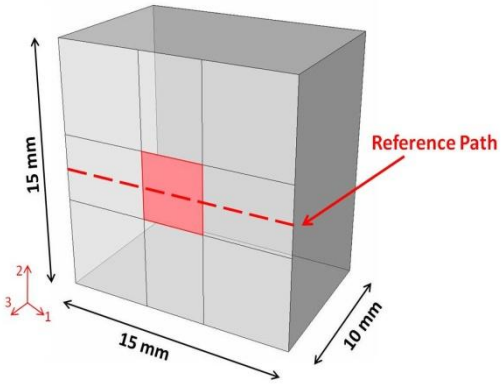

Figure 5-2 Single peen model for mesh sensitivity study

Only one shot peen has been applied and four different mesh sizes has been used to investigate them influence on the induced residual stresses.

Cubic mesh element with edge of 0.15 mm, 0.20 mm, 0.30 mm and 0.40 mm has been used. These elements are of type C3D8R where letter R at the end of the element name labels reduced-integrated elements. C3D8R is solid (continuum) brick elements with 8 nodes and 3 degrees of freedom for each nods (the three translations) with reduced integration.

More details about types and characteristics of the mesh elements can be found in Appendix A.

In Fig.5-3 (a) residual stress results of the four respective analyses can be compared. Different colored areas clearly highlighted the gap of residual stresses between the distinct models.

The amount of this gap can be easily measured in the curves plotted in Fig.5-3 (b) that report values of residual stresses along the red reference path underlined in Fig.5-2.

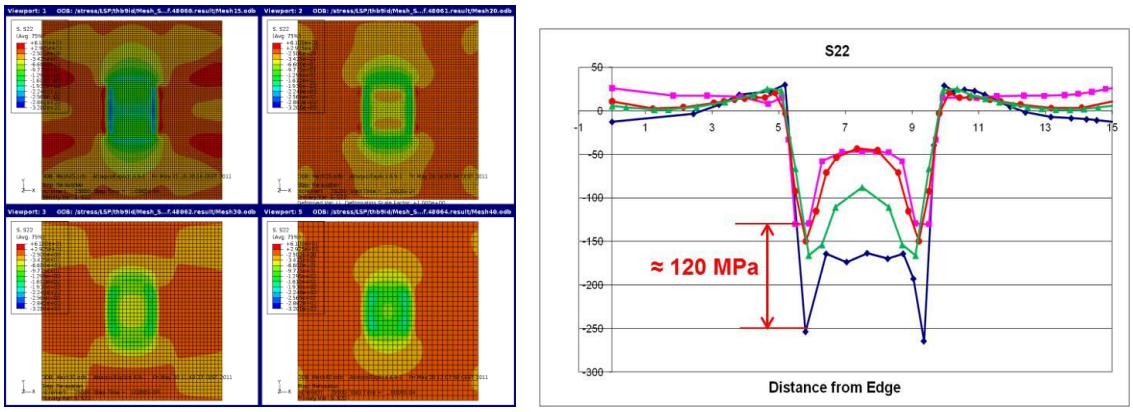

Figure 5-3 Differences of residual stress for the respective mesh element size

What is surprising is the measured gap exists not only between the peaks but even between the mean values and this cannot be explained as a simple capability of the finer mesh model to catch more details.

After these considerations a mesh optimization process started.

First of all it has been noticed that under the pressure load all the mesh elements are subjected to a strong deformation in the direction of the load, but only small deformations occur in the other two directions.

This phenomenon can be appreciated in Fig.5-4

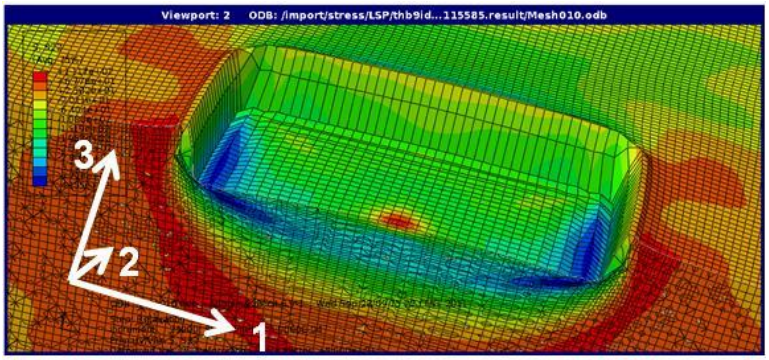

Figure 5-4 Typical mesh elements deformation under the pressure load

To prevent this kind of unwanted deformations a new shape of mesh element has been used with a three times smaller size in the load direction. Of course this reduction of the dimension implied a considerable increase of the global number of the elements. This increment has been paid with an "in plane" size increasing (and so number decreasing) of the same elements as can be seen in Fig.5-5.

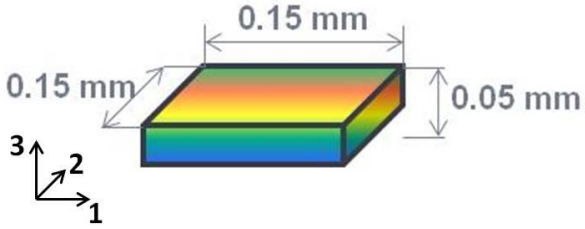

Figure 5-5 Mesh element optimized shape

All the investigations has been carried out over the simplified one peen model so to have a further reduction of the global number of the elements and to reduce the computational this refinement of the mesh has been done only in the peened area and in its surroundings. The same approach has been used in the load direction, where the finer mesh has been used only for a small thickness (in the order of the thickness affected by the laser peen), while for the remaining volume a coarser mesh has been used.
Similar strategy of mesh optimization can be found in [3] [4] and [5].
Fig.5- 6 shows the final simplified model with its dimensions and in Fig.5- 7 the mesh refinements have been highlighted while the peened area is the red one.

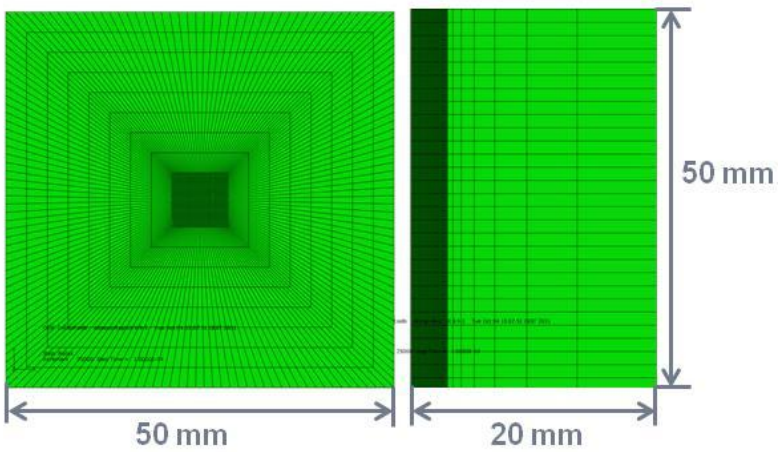

Figure 5-6 Final single peen model

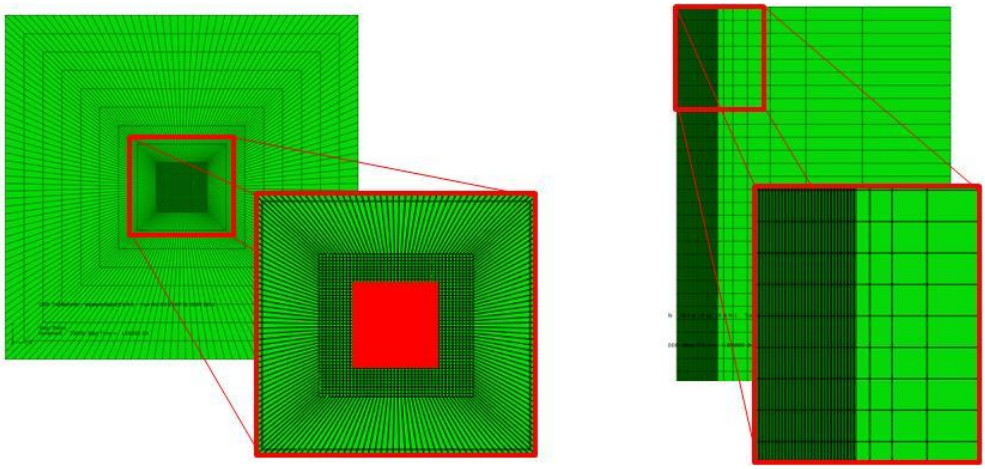

Figure 5-7 Mesh refinements in the model

Analyses with two difference mesh size has been carried out and values of stress, strain and plastic strain has been compared to prove that the mesh optimization process had a successful conclusion.

Fig.5-8 shows that for the three different measures the mean values of the two simulations are very similar. Dissimilarity can be noticed only in terms of peaks that, as already said, are due to the capability of the finer mesh to catch more details.

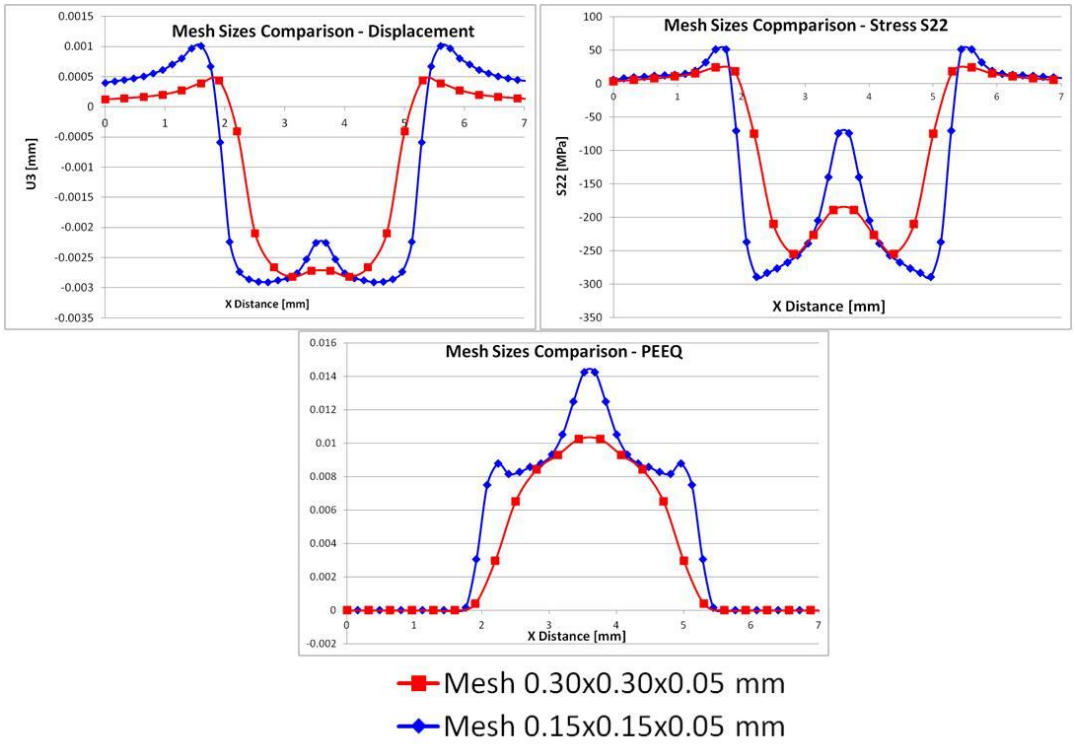

Figure 5-8 Comparison of displacement, stress and plastic strain for different optimized mesh elements sizes

5.3 Material Model Optimization

Once the mesh optimization process has been successful carried out and the uncertainty related to the instability of the mesh elements were removed, a new investigation on the material model parameters has been carried out.

5.3.1 Linear Elastic Investigation and Bulk Viscosity Tuning

First of all the elastic behavior of the material has been investigated to ensure one again that the analysis worked correctly and no other effects could influence the results.
Unfortunately, as shown in Fig.5-9, the simulation run with the default values exhibited some strange results.
If the material is considered completely elastic, in fact, it's expected to be in perfect equilibrium at the end of the process and not to show any residual stress or displacement.

Blue lines in Fig.5-9 show instead the presence of some of the above mentioned quantities.

This phenomenon cannot agree to the physics and therefore must be corrected.

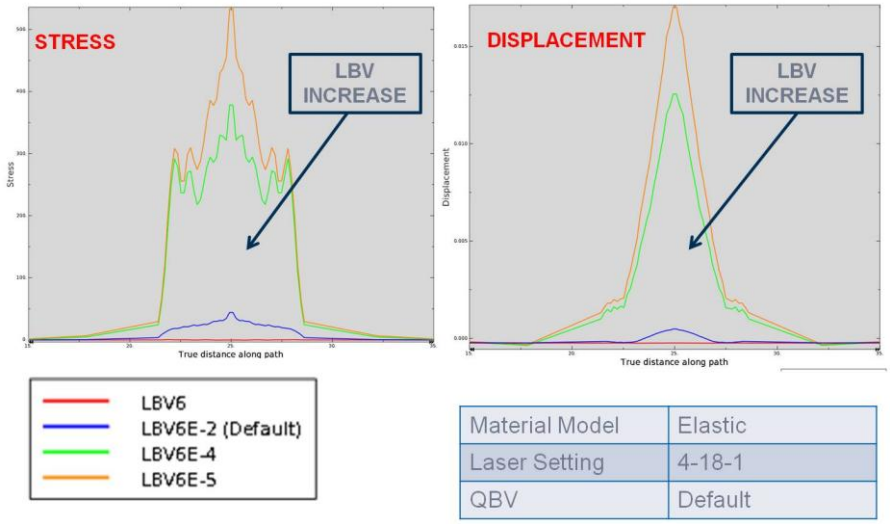

Figure 5-9 Results of linear elastic investigation

On this purpose the effect of the *Bulk Viscosity* parameters has been considered.

This quantity can be used in Abaqus/Explicit with two different parameters: *Linear Bulk Viscosity* (LBV) and *Quadratic Bulk Viscosity* (QBV) with which is possible to introduce damping associated with the volumetric straining [6].

More details about Bulk Viscosity can be found in Appendix B.

What can be deduced from Fig.5- 9 is that in the model was present a kind of instability related to the high frequency of the elements that led to a final state of non equilibrium. The equilibrium is in fact reached only with the use of a great amount of artificial damping introduced via the LBV parameter. The trend is confirmed because decreasing LBV under the default value of 0.06 the residual stress and displacement increased while only using a LBV equal to 6 (i.e. two order of magnitude greater than the default one) the complete equilibrium state is reached.

Moreover to guarantee a consistency of the simulation the QBV has been increased.

Hence from this point forward all the analyses have to be intended as performed with a LBV value equal to 6 and a QBV value equal to 1200.

5.3.2 Non-Linear Plastic Investigation

In chapter 5 has been already mentioned that JC's material model has been chosen as the most suitable to this kind of simulations.

The stress-strain relation is expressed by the following equation:

$$\sigma = [A + B\varepsilon^n]\left[1 + C \ln\frac{\dot{\varepsilon}}{\dot{\varepsilon_0}}\right][1 - T'^m] \quad (5.1)$$

As can be seen from (1) the key-factor of this material model is that the flow stress (σ) of the material are expressed as a product of three terms: strain hardening, strain rate and thermal dependence and the influence of each of them can be evaluated independently from the others.

However the correct estimation of all the parameters involved in (5.1) is a challenging procedure. They are, in fact, scarcely mentioned in literature while to determine it experimentally, tests on *split hopkinson bar* are needed. An example of determination of JC's parameters for Titanium can be found in [7] as a proof that the process is not trivial at all.

The parameters used in the previous investigations are the ones shown in Tab.1 and they have been found in literature in [2].

A [MPa]	**B [MPa]**	**n**	**C**	**ε_0**	**m**
490	207	0.344	0.005	1	1.8

Tab. 5-1 JC Parameters used in previous investigations

The analysis of these JC parameters, however, showed a discontinuity between the linear and the non-linear curve after the yield strength for the material taken into account as shown in Fig.5-10.

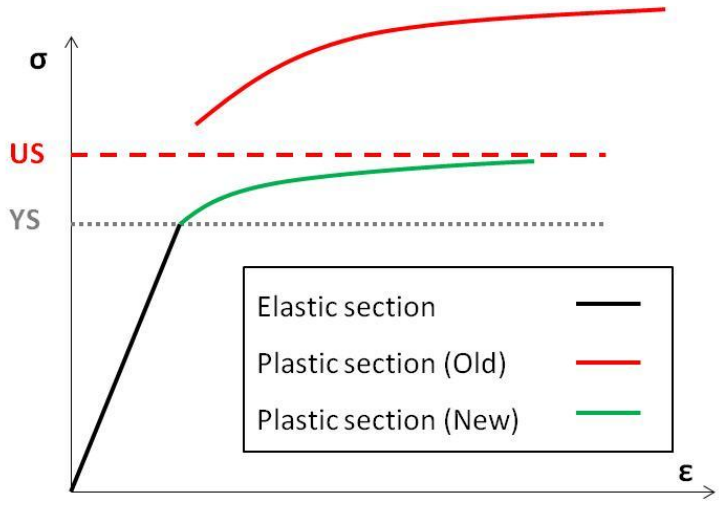

Figure 5-10 Stress-strain relation for old and new JC parameters

A modification of the parameters was therefore necessary to restore the continuity.
The new parameters are reported in Tab. 5-2

A [MPa]	**B [MPa]**	**n**	**C**	**ε_0**	**m**
435	110	0.03	0.001	1e+06	1.8

Tab. 5-2 New JC parameters

Further simulations with the new JC parameters has been done even to verify if the point of application of the artificial damping could have any influence.
Results of these analyses are shown in Fig.5-12 where every line represents the residual displacement measured along the reference path in Fig.5-11.

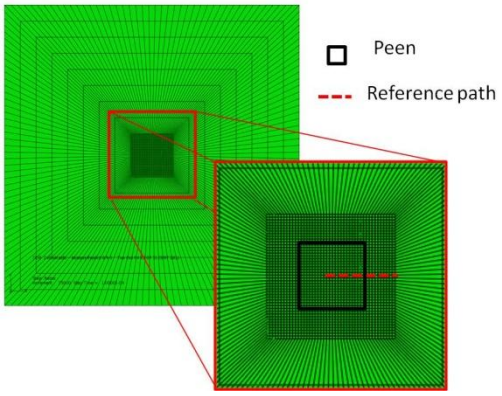

Figure 5-11 Reference path in the model

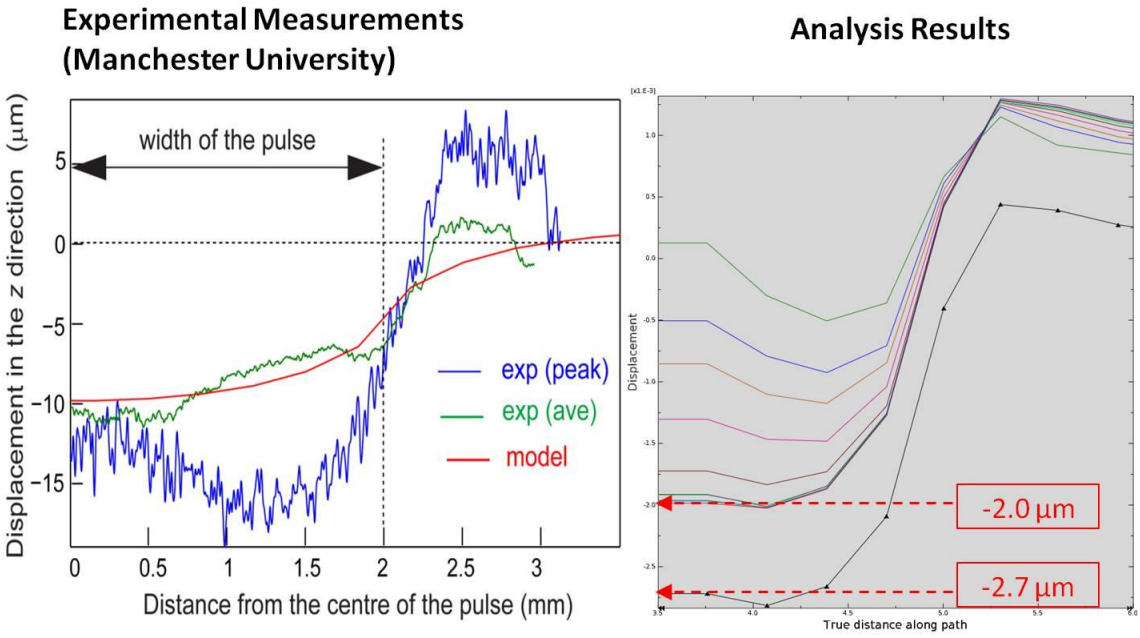

Figure 5-12 Analysis Results and comparison with experimental results [8]

Fig.5-12 shows also the direct comparison in terms of displacement between the analysis results and the experimental one coming from Oxford University [8]. Even if the global trend is confirmed, a big gap exists between the experimental and the numerical values that even with the nee JC's parameters and the bulk viscosity correctly tuned cannot go further than -2.7 µm.

To feel this gap and to calibrate the numerical model several parameters in the material equation has been modified but the only one that seems effectively influencing the displacement is the yield strength.

Fig.5-13 shows, in fact, that choosing a material with a yield strength of 80MPa allows to have a good fit of the numerical curve with a resulting displacement of about -11.0 µm.

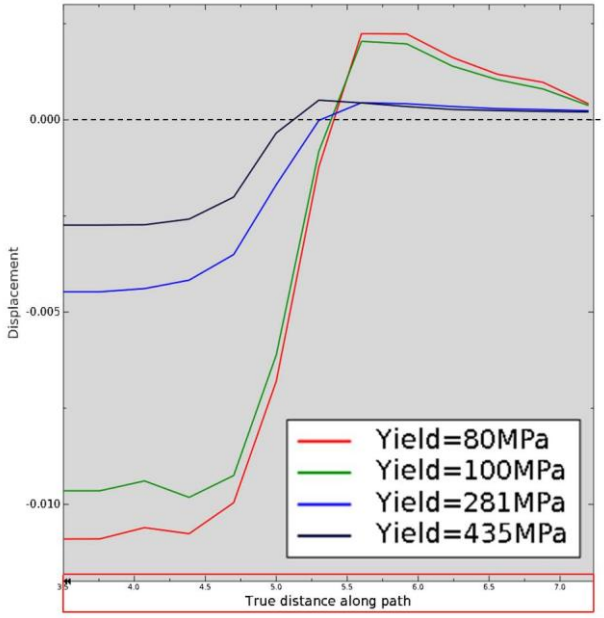

Figure 5-13 Residual displacement results varying yield stregth

This value of yield strength is however far away from the realistic one for the material of the coupon (AA7050-T7451), so this last analysis has been used only as a suggestion that probably simulation doesn't take into account some aspects related to the surface condition (temperature effect, ablative layer).

It must be remembered in that, unlike the complete simulation tool *ShockLas* described in §4.2.3, this analysis procedure models only the effect of the plasma pressure neglecting all the interactions between the plasma and material or the incidence of the laser itself.

The above mentioned considerations however led to think carefully to what happens at the surface of the coupon during the LSP process.

5.4 Ablative Layer Modeling

Fig.5-14 shows a test coupon peened by Metal Improvement Company in Earby.

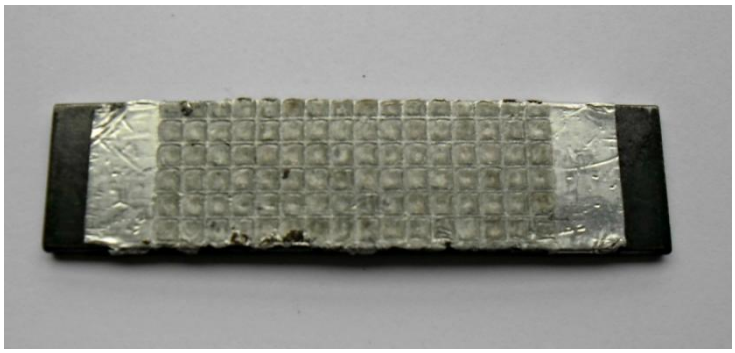

Figure 5-14 Laser Peened Coupon

MIC laser system consists in an output beam, roughly 25 Joules at 18 nanoseconds, from a Nd:glass laser that is projected onto the work piece. The area to be peened is covered, as shown, with aluminum foil of about 100 μm that acts as an ablative layer and simultaneously as a thermal insulating layer. A 1-3 mm layer of water is constantly flowing over the surface and constituted the so called tamping layer.

The pure aluminum foil is stuck on the coupon by means of a super thin layer of glue.

The aluminum foil and the glue constitute a layer made of a material with completely different properties from the one of the coupon. They are together generically called *ablative layer* to indicate that part of them evaporates during the process. However, as evident in Fig.5-14, ablative layer is never completely vanished and it is necessary to remove it manually at the end of the treatment.

To be as close as possible to the real dynamic of the phenomenon it has been decided to model even the ablative layer.

A perfectly-plastic material model has been used with a yield point of 10 MPa as indicated in [9] for pure aluminum while the presence of the glue has been considered negligible in terms of yield strength.

In the model the ablative layer has been realized as a simple 100 μm partition of the solid with total continuity condition at the interface between the two partitions.

Fig.5-15 shows the model including the ablative layer (red part) .

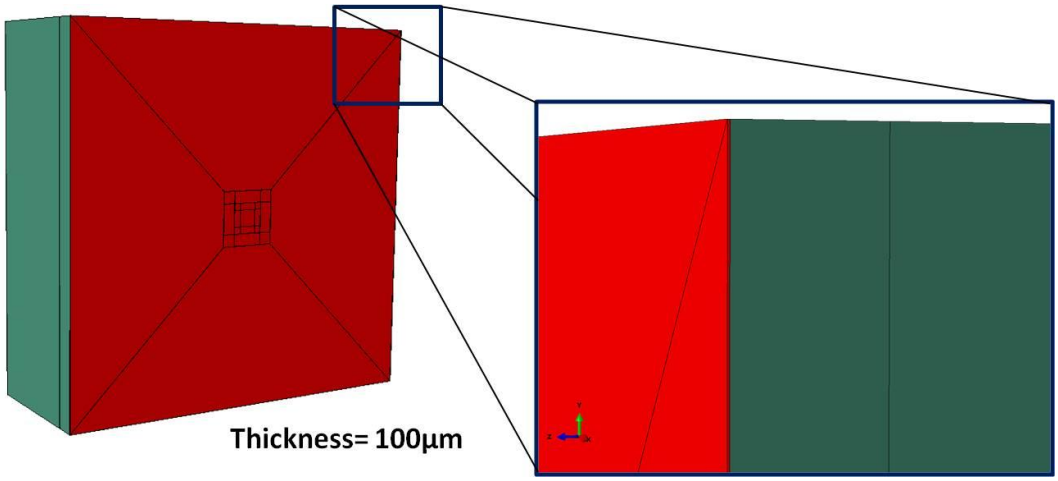

Figure 5-15 Ablative Layer Modeling

5.5 Laser Pulse Profile Optimization

In order to complete the optimization process and to have a model as close as possible to the real physic process, a refinement of the laser pulse profile simulation has been carried out as well.

5.5.1 Temporal Laser Pulse Profile

Fig.5-16 presents some examples of numerical simulations of shock wave decay in depth (0 and 457 µm) as a function of time for 25 ns FWHM (Full Width at Half Maximum) laser pulse duration and various power densities (2, 6, and 8 GW/cm^2) done by Berthe et al. in [10]. The pressure profile at a 0 µm depth corresponds to the pressure generated at the front surface of the target by a laser impact in the water confined regime. The shock wave is approximately two times longer than the laser pulse duration (about 50 ns versus 25 ns) due to the delayed cooling phase of the plasma (while the laser is switched off).

Due to this velocity difference between the elastic and plastic waves, the elastic release, coming back from the front surface of the target reduces the shock-wave amplitude.

In order to take into account this behavior of the shock wave, it has been decided to model the temporal profile of the laser pulse not simply as a triangle but with a more complex shape with two different amplitudes (as shown with the red line in Fig.5- 16).

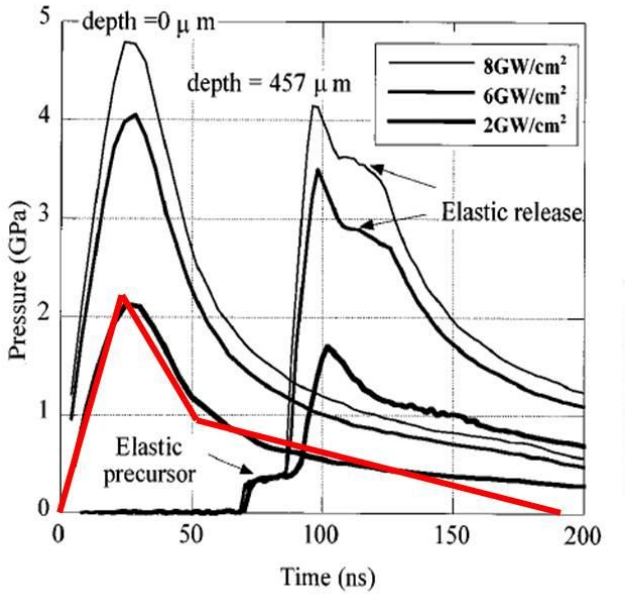

Figure 5-16 Simulations of the shock wave profiles done in [10]

The final setting of the analysis temporal steps is finally shown by Fig.5- 17.

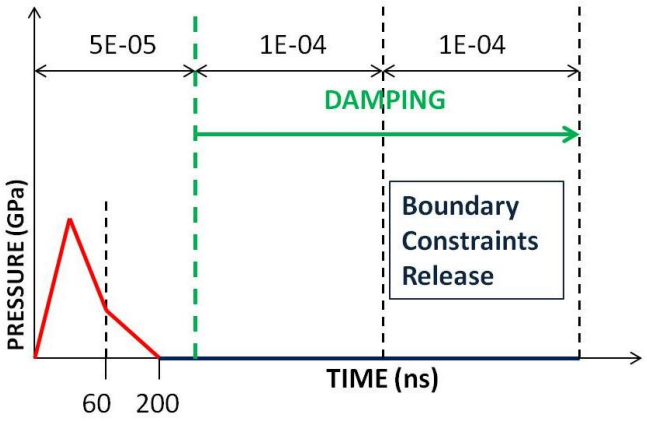

Figure 5-17 Analysis temporal steps

During the first step of the analysis the sample is subjected to the boundary conditions and the laser pressure is applied on it with a temporal profile described by the red line. The maximum pressure peak is calculated by the following equation given in [10]

$$P\ (GPa) = \ 1.02\sqrt{I_0(GW\ cm^{-2})} \qquad (5.2)$$

Of course during this first step no artificial damping is applied in order not to invalidate the plastic deformations.

Bulk viscosity acts only in the last two steps. In these steps the wave propagation and the spring back oscillations take place as a consequence respectively of load and boundary conditions release.

5.5.2 Spatial Laser Pulse Profile

As already mentioned in Chapter 5, for all the previous investigations a uniform spatial profile has been used.

The decreasing of the mesh element size, however, revealed discontinuity problems at the interface between the peened and the unpeened area. It must be considered, in fact, that the boundary sees an instantaneous pressure variation from zerp to thousand of MPa.

For this reason a new *distributed* profile has been applied as shown in the following pictures.

In Fig.5-18 it's possible to see the pressure peak that in previous works has been applied as a simple uniform step (blue line). In the new model it was first applied with a slope involving one element raw (red line) and then three elements raw (green line).

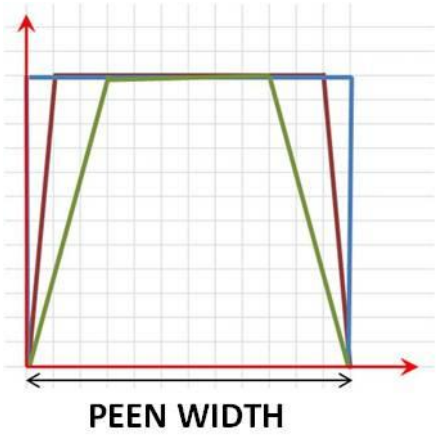

Figure 5-18 Distribution of pressure along peen width

The last solution has been chosen and Fig.5-19 shows the resulting pressure distribution with a colored gradient from blue (minimum) to red (maximum).

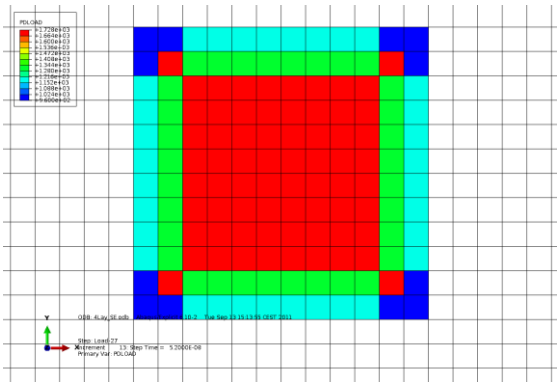

Figure 5-19 Pressure distribution on a peen surface

The advantage of using a so shaped spatial profile are quite evident from the curves in Fig.5-20 in which comparison between uniform and distributed profile for two different values of pressure peak are plotted.

As evident the trend and the mean value of the residual displacement along the path in Fig.5-11 is confirmed. However there is a big difference in terms of peaks: using a distributed spatial profile reduce the discontinuity at the peen boundary so a smoothed curve is obtained.

The influence of the spatial profile is more evident if the comparison is done in terms of stresses and not in terms of displacement.

More details can be found in the next §5.6.

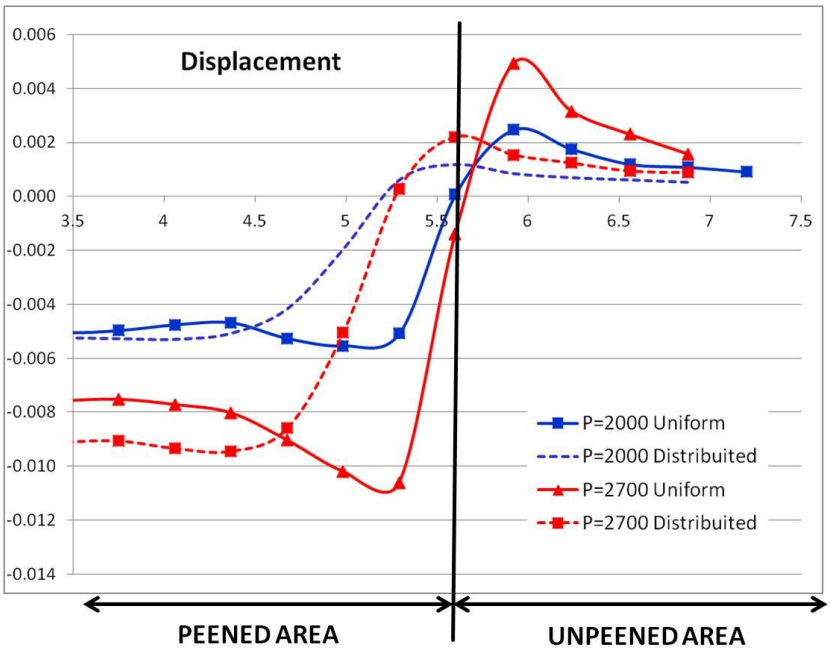

Figure 5-20 Comparison of Uniform and Distributed Spatial profile

5.6 Calibration with experimental Results

Once the optimization process finished and all the parameters were adjusted, a validation process has been carried out.

Calibration was made using experimental results for different laser settings, peening sequences and geometries.

5.6.1 Calibration with displacement measurements

Calibration in terms of displacement has been carried out for one-peen model and for two different laser settings : 2-18-1 and 3.2-18-1 where the first number stands for laser power density in GW/cm^2, the second one the pulse duration in nanoseconds, the third the number of laser layers.

Fig.5-21 shows a comparison between experimental results obtained from [8] and the two simulation strategies: eigenstrain method carried out at Oxford University and the Explicit method applied in this work.

The green line representing simulation done without ablative layer modeling is also reported in order to clarify the final rule of this strategy. It is possible to see, in fact, that the green line is far away from the experimental results.

It's furthermore needed to point out that all the measurements regarding the model with ablative layer has been done under the layer itself, exactly like what happen for real measurements in coupons.

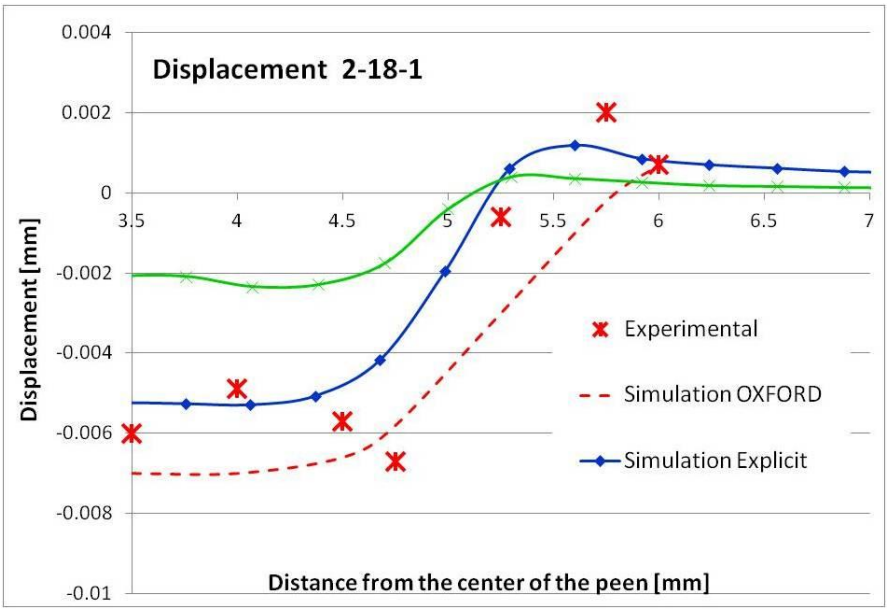

Figure 5-21 Numerical – experimental comparison of displacements for 2-18-1 laser configuration, measured along Fig. 5-11 path

The matching between simulation and experimental results verified for 2-18-1 configuration is also confirmed for 3.2-18-1 configuration and it can be appreciated in the following Fig.5-22.

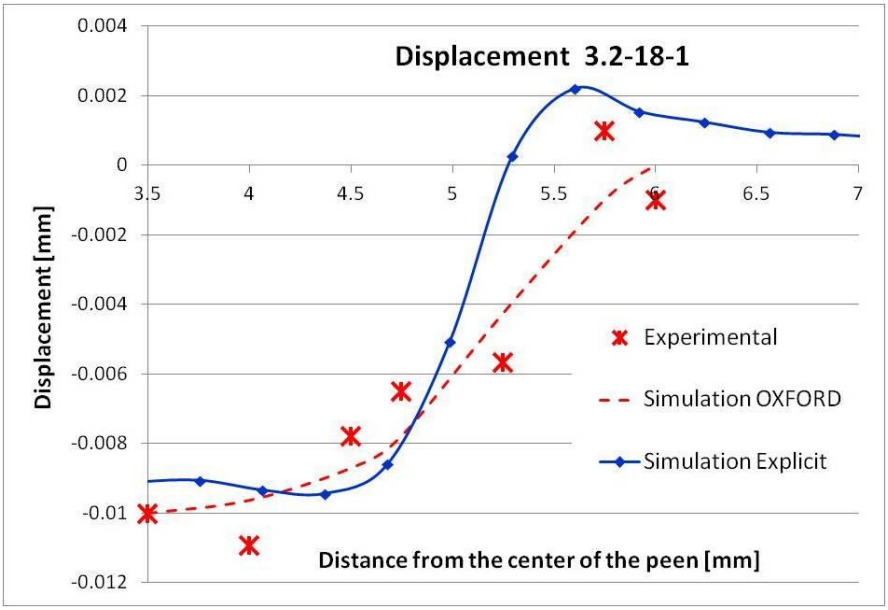

Figure 5-22 Numerical – experimental comparison of displacements for 3.2-18-1 laser configuration, measured along Fig. 5-11 path

5.6.2 Calibration with stress measurements

The good results obtained from the calibration in terms of displacement induced to be confident that stresses calibration shown in Figg. 5-23 and 5-24 could be fine as well.

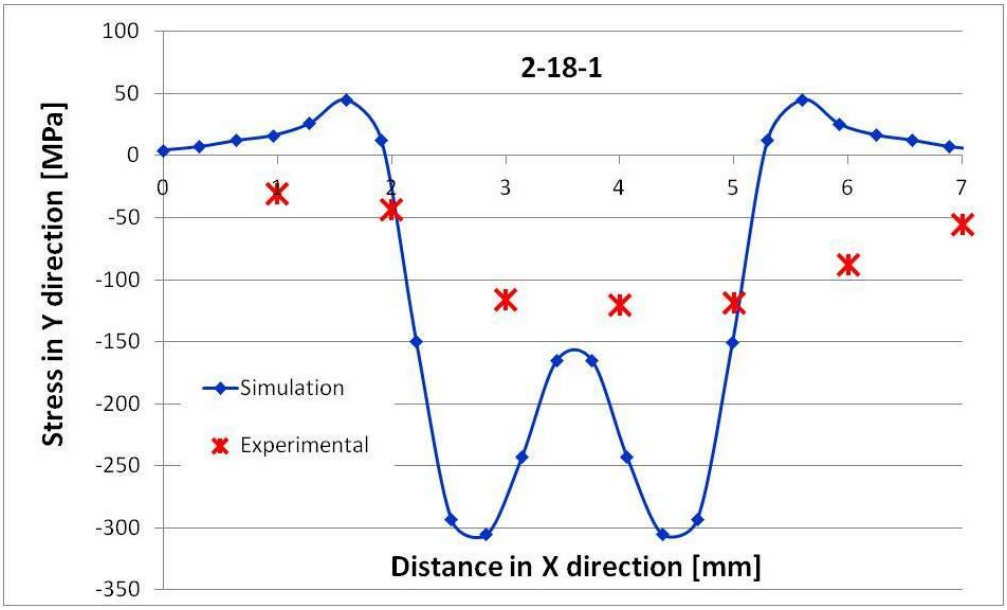

Figure 5-23 Numerical – experimental comparison of stress for 2-18-1 laser configuration, measured along Fig.5-11 path

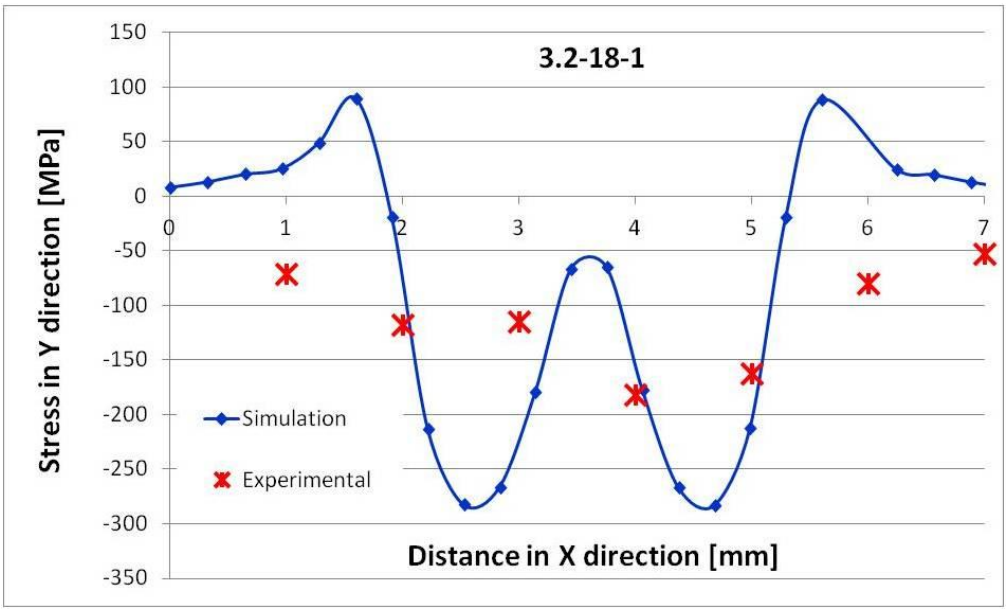

Figure 5-24 Numerical – experimental comparison of stress for 3.2-18-1 laser configuration, measured along Fig.5-11 path

At first sight it could appear that the matching in terms of stresses is not verified, however some thorny aspects must be taken into account.

First it must be noticed that the experimental measurements are available only in few points of the surface because of the intrinsic resolution of the measurements tool. The simulation instead is able to provide a continuous profile, therefore in some points of the surface it is not possible to say if the matching occur or not.

It is possible to consider however a sort of mean of the stress induced by the process and to perform an energy equivalence with the help of Fig.5-25.

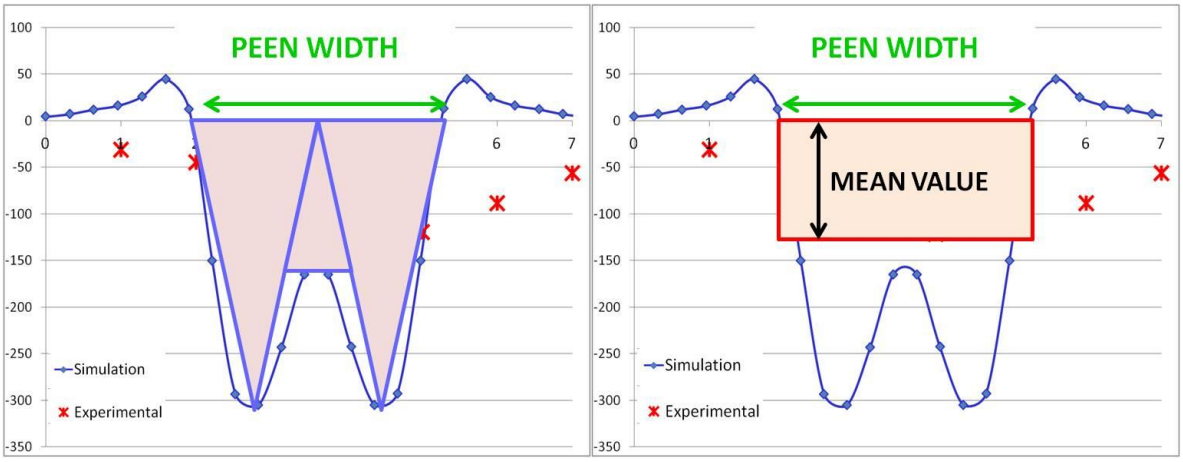

Figure 5-25 Energy Equivalence

Considering first the experimental results, it's possible to compute the area under the curve as the sum of three triangles areas (left part of Fig.5-25). This area can be redistributed as a rectangle uniform area with the basis corresponding to the peen width (right part of Fig.5-25).

Having the basis of the rectangle is then possible to compute the height of the same rectangle that allows it to have the same area of the triangles.

This height is equivalent to the mean value of the residual stresses and is verified in both cases to match the experimental results with respective values of -150 MPa and -178.5 MPa.

The unmatched global trend in spite of the comparable values of total energy can be justified considering the discontinuity in the simulation of a single laser spot.

5.6.3 Influence of multiple spots

Fig.5- 26 shows the results of a simulation done with three spot in line (only one layer). Colors clearly highlight that there are higher numerical discontinuities at the boundary between the peened and unpeened areas, while in the central peen a non critical situation occurs.

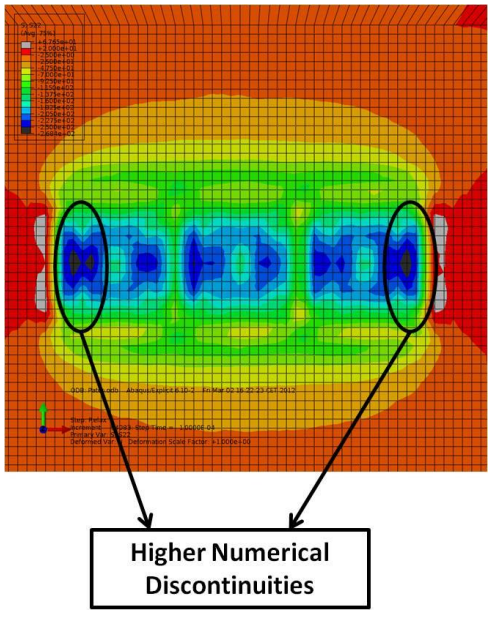

Figure 5-26 Abaqus stress field for 3 spots, 2-18-1 laser configurations

This stress state shows a trend more closer to the experimental results, as reported in Fig.5-27.

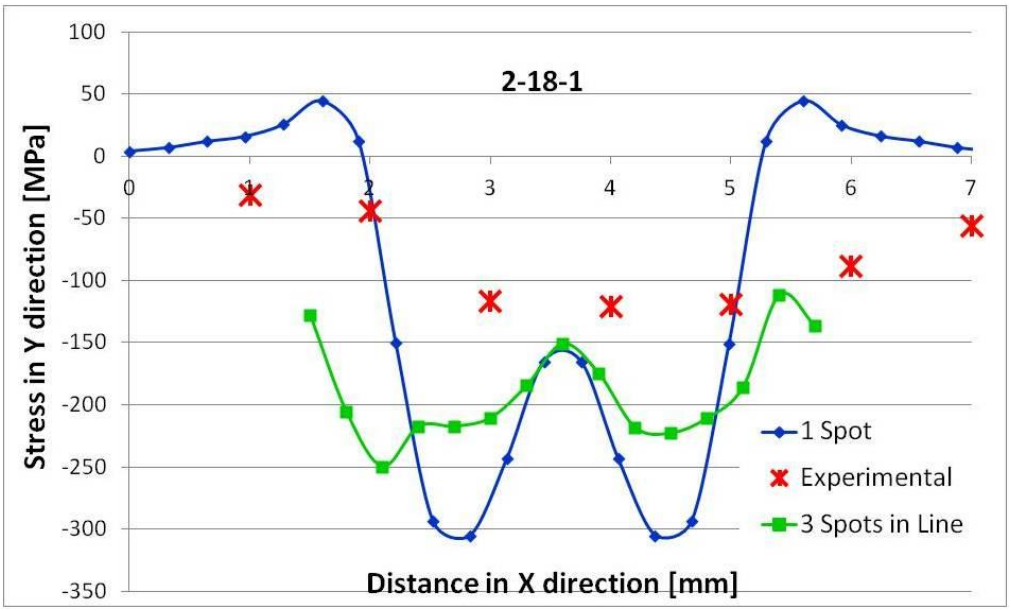

Figure 5-27 Numerical – experimental comparison of stresses for 2-18-1 laser configurations, measured along Fig.5-11 path

The residual stress peaks of the one spot model (blue line) are considerably reduced in the three spot simulations (green line) and the mean value is directly matched without the need of an energy equivalence.

5.6.4 Influence of multiple layers

Further calibrations has been done involving multiple layers and more complex geometries.

The design of the specimen in Fig.5-28 used for the experimental tests has been defined after an intensive research campaign developed by Airbus in collaboration with EADS-IW, in order to represent as best the structural conditions of the aircraft components. All the specimens has been sent to MIC in Earby (UK) for LSP treatment.

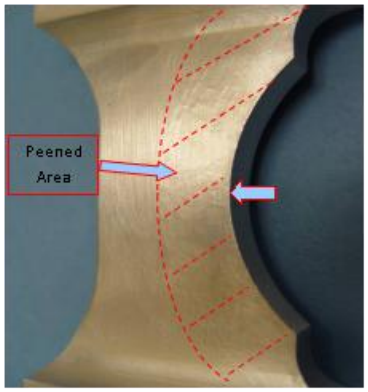

Figure 5-28 EADS-IW peened specimen [1]

Settings' data of the process have been provided from the company and they have been directly used for the simulations and the calibrations even in previous works like [1].

In the analysis, only the treated part that correspond to a parallelepiped with the real dimensions has been modeled, as already mentioned in Chapter 5.

All the simulations have been performed taking into account the presence of the ablative layer.

Several patches of laser spots have been overlaid on three faces of the specimen. Numerical results in terms of residual stresses have been compared with experimental measurements carried out in EADS-IW.

Two different reference paths, showed in Fig.5-29, have been taken into account.

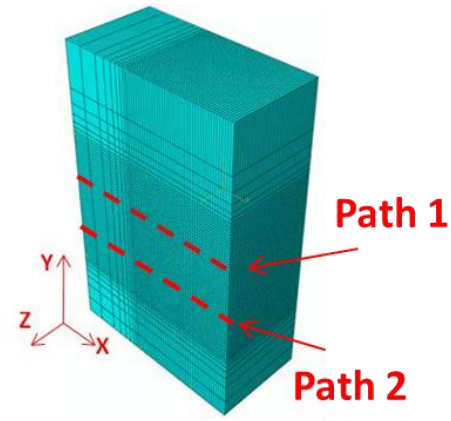

Figure 5-29 Reference paths

The result of the simulation compared with experimental results is shown in Fig.5-30 for 4-18-2 laser configuration. The comparison has been done with two peened specimens (1 and 2) with the same laser settings.

Is evident that the global trend of the residual stresses is confirmed, in particular in the peened area.

The small gap between simulation and tests present in the unpeened area (from 0 to 5 mm) is instead ascribed to the fact that real coupon already have residual stresses due to the machining while the numerical model is stress-free.

Is moreover interesting to notice that approaching the edge there is a drop of residual stresses as a consequence of the presence of less elastic material.

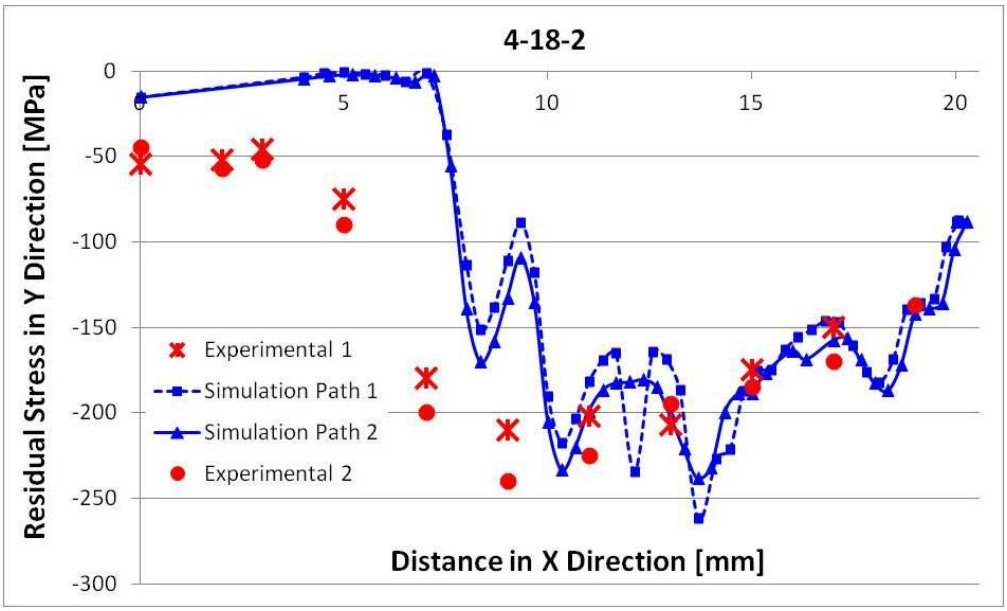

Figure 5-30 Numerical – Experimental comparison of stresses for 4-18-2 laser configuration

A further simulation with 2-18-4 laser settings has been carried out, even if no experimental data were available for this configurations.

It was however useful to have a look at the trend of this analysis to have the proof that peaks of discontinuities totally disappear for multiple layer configurations as shown in Fig.5- 31.

Moreover, the mean value of the stresses is realistic, considering that an increase of the laser shot layers beyond 3 is not affecting the surface stresses [11].

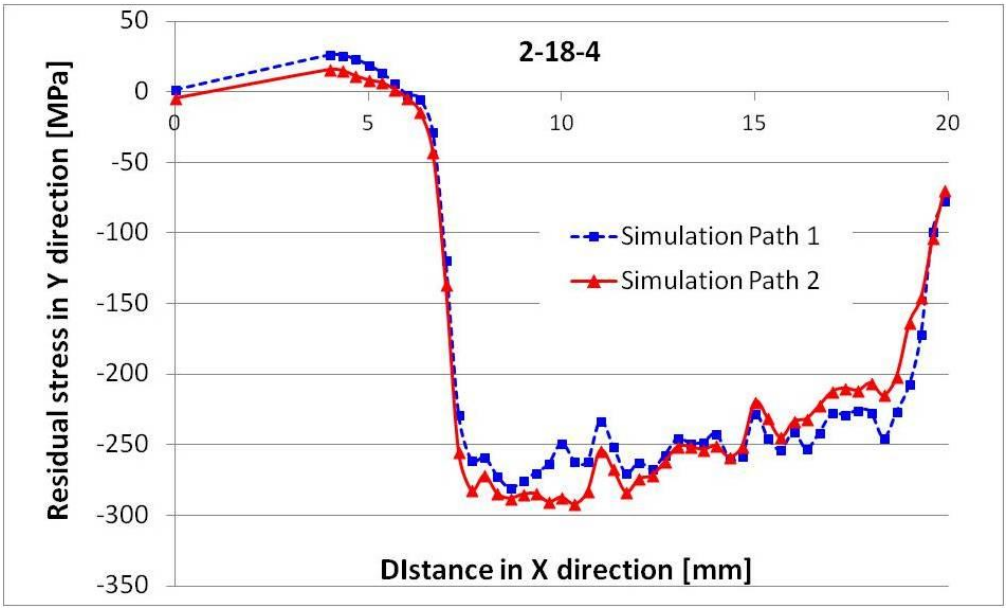

Figure 5-31 Numerical trend of stresses for 2-18-4 laser configurations

The good correlation of the numerical and experimental results has been verified for multiple-layers configuration even with in-depth measurements.

The layer configuration is shown in Fig.5-32, the grey area corresponds to the one modeled with a finer mesh and the blue areas are the overlapped peens, shifted of about 75%, so the 300% covered area is the one bounded by the white line.

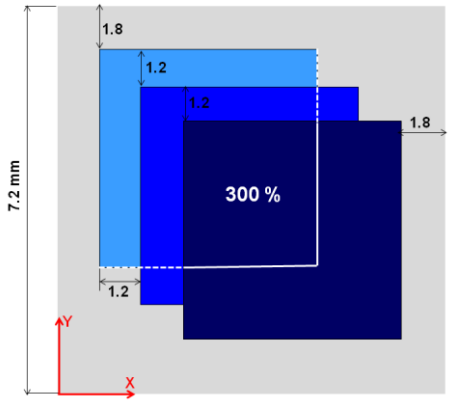

Figure 5-32 Layers Configurations

Comparisons with numerical results and experimental measurements done by EADS-IW are shown in Fig.5-33. The experimental data shows a gap from the surface to the first 0.2mm because for surface measurements XRD tool has been used, while in depth measurements have been done with ICHD method that cannot reach the surface.

A good fitting of the numerical results is verified also in this case, with the further advantage that by simulation results for all depth distance can be obtained, while the experimental measurements are limited by the sensitivity of the instrumental tools.

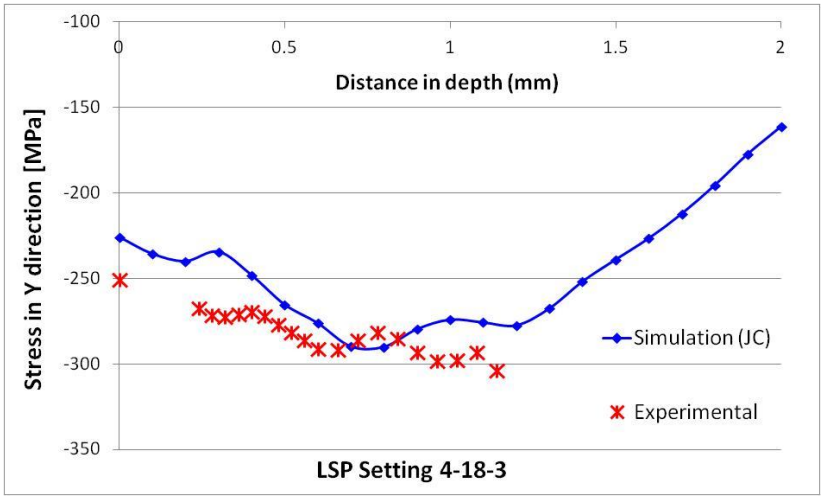

Figure 5-33 Numerical – Experimental comparison of "in depth" stresses for 4-18-3 laser configuration

5.7 Bibliography – Chapter 5

[1] M.Sticchi, "Finite element modelling of Laser Shock peening-Geometrical Constraints Impact on Residual Stress Distribution After Laser Shock Peening". (2011). University of Neaples "Federico II".

[2] Liu Zhanqiang, Shi Zhenyu and Guo Yuebin, “Fem Simulation of Minimum Uncut Chip Thickness in Mechanical Microcutting”;(2006) ISMNM 2010 – Guilin and Han et al.

[3] W. Braisted, R. Brockman, "Finite element simulation of laser shock peening".(1998). International Journal of Fatigue 21 (1999) 719-724

[4] K. Ding, L. Ye, "Three dimensional dynamic finite element analysis of multiple laser shock peening processes". (2002). Surface engineering Vol.19 n°5 (2003) 351-358

[5] M. Achinta, D. Nowell, "Eigenstrain modeling of residual stresses generated by laser shock peening". (2010). Journal of materials processing technology 211(2011) 1091-1101

[6] Dassault Sistèmes. "Explicit Dynamic Analysis ". Abaqus/CAE User's Manual. (2011). Vol. II §6.3.3

[7] A.Dorogoy, D.Rittel. "Determination of the Johnson-Cook material parameters using the SCS specimen". (2008). Experimental Mechanics December 2009, Volume 49, Issue 6, pp 881-885.

[8] Shapiro, K., Achintha, M., Nowell D. and Withers, P.J. (2011). In: Proceedings of the Third International Conference on Laser Peening and related phenomena, Osaka, Japan

[9] G.E.Totten, D.Scott MacKenzie. "Handbook of Aluminum". Vol.1 Physical Metallurgy and Processes. (2003). Marcel Dekker Inc. New York.

[10] L. Berthe, R. Fabbro, P. Peyre, L. Tollier, and E. Bartnicki. "Shock waves from a water-confined laser-generated plasma". (1997). J. Appl. Phys. 82, 2826 (1997).

[11] Peyre P, Fabbro R, Merrien, P. and Lieurade, H.P. " Laser shock processing of aluminium alloys. Application to high
cycle fatigue behaviour ". (1996). Material Science and Engineering , A210 (1996) 102-113

Chapter 6

6 Conclusions and Further Studies

6.1 Conclusions

From the results of the present work, LSP is confirmed as an effective method to introduce significant compressive residual stresses in fatigue sensitive areas of metallic structures, postponing fatigue crack nucleation.

The application of the numerical FE simulation to LSP showed to be extremely difficult as a consequence of the parameters involved in the process. An optimized ABAQUS/Explicit model was developed and calibrated by means of experimental results.

The numerical investigations led to a more controllable and reliable finite element model, valid even for complex geometries.

Moreover, the study about the material properties highlighted a gap of the standard models about the simulation of the surface conditions. The solution was in the modeling of the ablative layer employed during the real process, usually a super thin sheet of pure aluminum stuck on the masterpiece. In the simulation, it has been reproduced as a 100μm layer made by a material with a yield point of 10MPa.

Spatial and temporal laser pulse modeling has been improved as well to reduce as much as possible the numerical discontinuities.

All those new settings have been applied to a set of analyses made with different geometry models to verify the robustness of the model. The calibration of the model with experimental results was based on stress and displacement measurements.

Displacement calibrations showed an excellent correlation between experimental and numerical results, while stress calibrations highlighted numerical discontinuities problems that however disappear in multiple spots or multiple layers configurations.

Simulations globally show good fitting of the experimental results proving this model to be reliable for prediction of detailed effects of LSP.

6.2 Further Studies

Modeling the ablative layer seemed to be the key-point of the success of these analyses.

However the material model used for the ablative layer is not optimized yet. A better estimation of the material characteristics of this layer, including the presence of the glue and the variation in terms of impedance, will ensure the model to be more reliable.

Once the all-round optimization process could be considered finished, will be useful to implement some Python scripts to automatize the preprocessing and to reduce the global time-costs of the simulation.

In this way could be possible to have a sort of catalogue of residual stresses for respective laser settings and geometrical configurations that could be used coupled with eigenstrain method or Abaqus/Standard analyses.

A so built model could definitively represent a powerful tool for predicting residual stresses and consequently for determining the laser-geometry configuration that maximize the fatigue life enhancement.

Application in laser forming process planning will be advantageous as well.

APPENDIX A

A.Mesh Elements and Integration overview

A.1 Mesh elements overview

(ref..Abaqus 6.11 Analysis User's Manual Vol. IV sect. 26.1.1. Dassault Sistèmes)

Abaqus has an extensive element library to provide a powerful set of tools for solving many different problems.

Five aspects of an element characterize its behavior:

- Family
- Degrees of freedom (directly related to the element family)
- Number of nodes
- Formulation
- Integration

Each element in Abaqus has a unique name, such as T2D2, S4R, C3D8I, or C3D8R. The element name identifies each of the five aspects of an element. For details on defining elements.

Family

Figure A–1 shows the element families that are used most commonly in a stress analysis; in addition, continuum (fluid) elements are used in a fluid analysis. One of the major distinctions between different element families is the geometry type that each family assumes.

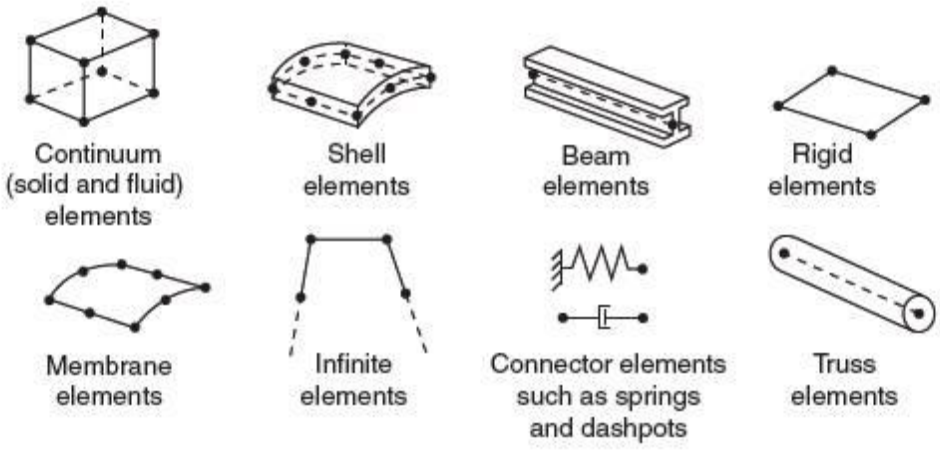

Figure A-1 Commonly used element families

First letter or letters of an element's name indicate to which family the element belongs. For example, S4R is a shell element, CINPE4 is an infinite element, and C3D8I is a continuum element.

Degrees of freedom

The degrees of freedom are the fundamental variables calculated during the analysis. For a stress/displacement simulation the degrees of freedom are the translations and, for shell, pipe, and beam elements, the rotations at each node. For a heat transfer simulation the degrees of freedom are the temperatures at each node; for a coupled thermal-stress analysis temperature degrees of freedom exist in addition to displacement degrees of freedom at each node. Heat transfer analyses and coupled thermal-stress analyses therefore require the use of different elements than does a stress analysis since the degrees of freedom are not the same. (See "Conventions," Section 1.2.2, of Abaqus AnalysisUser's Manual for a summary of the degrees of freedom available in Abaqus for various element and analysis types.)

Number of nodes and order of interpolation

Displacements or other degrees of freedom are calculated at the nodes of the element. At any other point

in the element, the displacements are obtained by interpolating from the nodal displacements. Usually

the interpolation order is determined by the number of nodes used in the element.

- Elements that have nodes only at their corners, such as the 8-node brick shown in Figure A–2(a), use linear interpolation in each direction and are often called linear elements or first-order elements.
- In Abaqus/Standard elements with midside nodes, such as the 20-node brick shown in Figure A–2(b), use quadratic interpolation and are often called quadratic elements or second-order elements.
- Modified triangular or tetrahedral elements with midside nodes, such as the 10-node tetrahedron shown in Figure A–2(c), use a modified second-order interpolation and are often called modified or modified second-order elements.

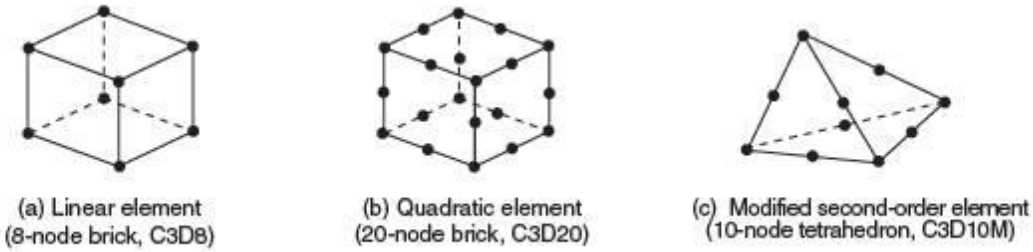

Figure A-2 Linear brick, quadratic brick, and modified tetrahedral elements

Typically, the number of nodes in an element is clearly identified in its name. The 8-node brick element is called C3D8, and the 4-node shell element is called S4R.

The beam element family uses a slightly different convention: the order of interpolation is identified in the name. Thus, a first-order, three-dimensional beam element is called B31, whereas a second-order, three-dimensional beam element is called B32. A similar convention is used for axisymmetric shell and membrane elements.

Formulation

An element's formulation refers to the mathematical theory used to define the element's behavior. In the Lagrangian, or material, description of behavior the element deforms with the material. In the alternative Eulerian, or spatial, description elements are fixed in space as the material flows through them. Eulerian methods are used commonly in fluid mechanics simulations. Abaqus/Standard uses Eulerian elements to model convective heat transfer. Abaqus/Explicit also offers multimaterial Eulerian elements for use

in stress/displacement analyses. Adaptive meshing in Abaqus/Explicit combines the features of pure Lagrangian and Eulerian analyses and allows the motion of the element to be independent of the material (see "ALE adaptive meshing: overview," Section 12.2.1 Abaqus AnalysisUser's Manual). All other stress/displacement elements in Abaqus are based on the Lagrangian formulation. In Abaqus/Explicit the Eulerian elements can interact with Lagrangian elements through general contact (see "Eulerian analysis," Section 14.1.1 Abaqus AnalysisUser's Manual).

To accommodate different types of behavior, some element families in Abaqus include elements with several different formulations. For example, the conventional shell element family has three classes: one suitable for general-purpose shell analysis, another for thin shells, and yet another for thick shells. In addition, Abaqus also offers continuum shell elements, which have nodal connectivities like continuum elements but are formulated to model shell behavior with as few as one element through the shell thickness.

Some Abaqus/Standard element families have a standard formulation as well as some alternative formulations. Elements with alternative formulations are identified by an additional character at the end of the element name. For example, the continuum, beam, and truss element families include members with a hybrid formulation (to deal with incompressible or inextensible behavior); these elements are identified by the letter H at the end of the name (C3D8H or B31H).

Abaqus/Standard uses the lumped mass formulation for low-order elements; Abaqus/Explicit uses the lumped mass formulation for all elements. As a consequence, the second mass moments of inertia can deviate from the theoretical values, especially for coarse meshes.

Abaqus/CFD uses hybrid elements to circumvent well known div-stability issues for incompressible flow. Abaqus/CFD also permits the addition of degrees of freedom based on procedure settings such as the optional energy equation and turbulence models.

Integration

Abaqus uses numerical techniques to integrate various quantities over the volume of each element, thus allowing complete generality in material behavior. Using Gaussian quadrature for most elements, Abaqus evaluates the material response at each integration point in each element. Some continuum elements in Abaqus can use full or reduced integration, a choice that can have a significant effect on the accuracy of the element for a given problem.

Abaqus uses the letter R at the end of the element name to label reduced-integration elements. For example, CAX4R is the 4-node, reduced-integration, axisymmetric, solid element.

Shell, pipe, and beam element properties can be defined as general section behaviors; or each cross-section of the element can be integrated numerically, so that nonlinear response associated with nonlinear material behavior can be tracked accurately when needed. In addition, a composite layered section can be specified for shells and, in Abaqus/Standard, three-dimensional bricks, with different materials for each layer through the section.

A.2 Integration of homogeneous solids

(ref. Abaqus 6.11 Theory Manual sect. 3.2.4)

All the isoparametric solid elements are integrated numerically. Two schemes are offered: "full" integration and "reduced" integration. For the second-order elements Gauss integration is always used because it is efficient and it is especially suited to the polynomial product interpolations used in these elements. For the first-order elements the single-point reduced-integration scheme is based on the "uniform strain formulation": the strains are not obtained at the first-order Gauss point but are obtained
as the (analytically calculated) average strain over the element volume. The uniform strain method, first published by Flanagan and Belytschko (1981), ensures that the first-order reduced-integration elements pass the patch test and attain the accuracy when elements are skewed. Alternatively, the "centroidal strain formulation," which uses 1-point Gauss integration to obtain the strains at the element center, is also available for the 8-node brick elements in Abaqus/Explicit for improved computational efficiency.
The differences between the uniform strain formulation and the centroidal strain formulation can be shown as follows:
For the 8-node brick elements the interpolation function given above can be rewritten as

$$\boldsymbol{u} = N^I(g,h,r)\boldsymbol{u}^I \quad \textit{sum on } I \tag{A.1}$$

The isoparametric shape functions N^I can be written as

$$N^I(g,h,r) = \frac{1}{8}\Sigma^I + \frac{1}{4}g\Lambda_1^I + \frac{1}{4}h\Lambda_2^I + \frac{1}{4}r\Lambda_3^I + \frac{1}{2}hr\Gamma_1^I + \frac{1}{2}gr\Gamma_2^I + \frac{1}{2}gh\Gamma_3^I + \frac{1}{2}ghr\Gamma_4^I \quad \text{(A.2)}$$

where

$$\Sigma^I = [+1,+1,+1,+1,+1,+1,+1,+1,] \quad \text{(A.3)}$$

$$\Lambda_1^I = [-1,+1,+1,-1,-1,+1,+1,-1,] \quad \text{(A.4)}$$

$$\Lambda_2^I = [-1,-1,+1,+1,-1,-1,+1,+1,] \quad \text{(A.5)}$$

$$\Lambda_3^I = [-1,-1,-1,-1,+1,+1,+1,+1,] \quad \text{(A.6)}$$

$$\Gamma_1^I = [+1,+1,-1,-1,-1,-1,+1,+1,] \quad \text{(A.7)}$$

$$\Gamma_2^I = [+1,-1,-1,+1,-1,+1,+1,-1,] \quad \text{(A.8)}$$

$$\Gamma_3^I = [+1,-1,+1,-1,+1,-1,+1,-1,] \quad \text{(A.9)}$$

$$\Gamma_4^I = [-1,+1,-1,+1,-1,+1,-1,+1,] \quad \text{(A.10)}$$

and the superscript *I* denotes the node of the element. The last four vectors, Γ_α^I (has a range of four), are the hourglass base vectors, which are the deformation modes associated with no energy in the 1-point integration element but resulting in a nonconstant strain field in the element.

In the uniform strain formulation the gradient matrix $\boldsymbol{B}^I$ is defined by integrating over the element as

$$B_i^I = \frac{1}{V_{el}}\int_{V_{el}} N_i^I(g,h,r)dV_{el}\,, \quad \text{(A.11)}$$

$$N_i^I(g,h,r) = \frac{\partial N^I}{\partial x_i} \quad \text{(A.12)}$$

where V_{el} is the element volume and *i* has a range of three.

In the centroidal strain formulation the gradient matrix $\boldsymbol{B}^I$ is simply given as

$$B_i^I = N_i^I(0,0,0), \quad \text{(A.13)}$$

which has the following antisymmetric property:

$$B_i^1 = -B_i^7 \quad \text{(A.14)}$$

$$B_i^3 = -B_i^5 \quad \text{(A.15)}$$

$$B_i^2 = -B_i^8 \quad \text{(A.16)}$$

$$B_i^4 = -B_i^6. \quad \text{(A.17)}$$

It can be seen from the above that the centroidal strain formulation reduces the amount of effort required to compute the gradient matrix. This cost savings also extends to strain and element nodal force calculations because of the antisymmetric property of the gradient matrix. However, the centroidal strain formulation is less accurate when the elements are skewed. For two-dimensional plane elements and hexahedron elements in a parallelepiped configuration the uniform strain approach is identical to the centroidal strain approach.

Full integration means that the Gauss scheme chosen will integrate the stiffness matrix of an element with uniform material behavior exactly if the Jacobian of the mapping from the isoparametric coordinates to the physical coordinates is constant throughout the element; this means that opposing element sides or faces in three-dimensional elements must be parallel and, in the case of the second-order elements, that the midside nodes must be at the middle of the element sides. If the element does not satisfy these conditions, full integration is not exact because some of the terms in the stiffness are of higher order than those that are integrated exactly by the Gauss scheme chosen. Such inaccuracy in the integration does not appear to be detrimental to the element's performance. As will be discussed below, full integration in Abaqus in first-order elements includes a further approximation and is more accurately called "selectively reduced integration."

Reduced integration usually means that an integration scheme one order less than the full scheme is used to integrate the element's internal forces and stiffness. Superficially this appears to be a poor approximation, but it has proved to offer significant advantages. For second-order elements in which the isoparametric coordinate lines remain orthogonal in the physical space, the reduced-integration points have the Barlow point property (Barlow, 1976): the strains are calculated from the interpolation functions with higher accuracy at these points than anywhere else in the element. For first-order elements the uniform strain method yields the exact average strain over the element volume. Not only is this important with respect to the values available for output, it is also significant when the constitutive model is nonlinear, since the strains passed into the constitutive routines are a better representation of the actual strains.

Reduced integration decreases the number of constraints introduced by an element when there are internal constraints in the continuum theory being modeled, such as incompressibility, or the Kirchhoff transverse shear constraints if solid elements are used to analyze bending problems. In such applications fully integrated elements will "lock"—they will exhibit response that is orders of magnitude too stiff, so the results they provide are quite unusable. The reduced-integration version of the same element will often work well in such cases.

Finally, reduced integration lowers the cost of forming an element; for example, a fully integrated, second-order, 20-node three-dimensional element requires integration at 27 points, while the reduced integration version of the same element only uses 8 points and, therefore, costs less than 30% of the fully integrated version. This cost savings is especially significant in cases where the element formation costs dominate the overall costs, such as problems with a relatively small wave-front and problems in which the constitutive models require lengthy calculations. The deficiency of reduced integration is that, except in one dimension and in axisymmetric geometries modeled with higher than first-order elements, the element stiffness matrix will be rank deficient. This most commonly exhibits itself in the appearance of singular modes ("hourglass modes") in the response. These are nonphysical response modes that can grow in an unbounded way unless they are controlled. The reduced-integration second order serendipity interpolation elements in two dimensions—the 8-node quadrilaterals—have one such mode, but it is benign because it cannot propagate in a mesh with more than one element. The second order three-dimensional elements with reduced integration have modes that can propagate in a single stack of elements. Because these modes rarely cause trouble in the second-order elements, no special techniques are used in Abaqus to control them.

In contrast, when reduced integration is used in the first-order elements (the 4-node quadrilateral and the 8-node brick), hourglassing can often make the elements unusable unless it is controlled. In Abaqus the artificial stiffness method and the artificial damping method given in Flanagan and Belytschko (1981) are used to control the hourglass modes in these elements. The artificial damping method is available only for the solid and membrane elements in Abaqus/Explicit. To control the hourglass modes, the hourglass shape vectors, γ_α^I , are defined:

$$\gamma_\alpha^I = \Gamma_\alpha^I - \frac{1}{V_{el}} B_i^I x_i^J \Gamma_\alpha^J \ , \qquad \text{(A.18)}$$

which are different from the hourglass base vectors, . It is essential to use the hourglass shape vectors rather than the hourglass base vectors to calculate the hourglass-resisting forces to ensure that these forces are orthogonal to the linear displacement field and the rigid body field (see Flanagan and Belytschko (1981) for details). However, using the hourglass base vectors to calculate the hourglass-resisting forces may provide computational speed advantages. Therefore, for the 8-node brick elements Abaqus/Explicit provides the option to use the hourglass base vectors in calculating the hourglass-resisting forces. For hexahedron elements in a parallelepiped configuration the hourglass shape vectors are identical to the hourglass base vectors.

The hourglass control methods of Flanagan and Belytschko (1981) are generally successful for linear and mildly nonlinear problems but may break down in strongly nonlinear problems and, therefore, may not yield reasonable results. Success in controlling hourglassing also depends on the loads applied to the structure. For example, a point load is much more likely to trigger hourglassing than a distributed

load. Hourglassing can be particularly troublesome in eigenvalue extraction problems: the low stiffness of the hourglass modes may create many unrealistic modes with low eigenfrequencies.

A refinement of the Flanagan and Belytschko (1981) hourglass control method that replaces the artificial stiffness coefficients with those derived from a three-field variational principle is available in Abaqus/Explicit. The approach is based on the enhanced assumed strain and physical hourglass control methods proposed in Engelmann and Whirley (1990), Belytschko and Bindeman (1992), and Puso (2000). It can provide increased resistance to hourglassing for nonlinear problems and coarse mesh displacement solution accuracy for linear elastic problems at a small additional computational cost.

Experience suggests that the reduced-integration, second-order isoparametric elements are the most cost-effective elements in Abaqus for problems in which the solution can be expected to be smooth. Note that in the case of incompressible material behavior, such as hyperelasticity at finite strain, the mixed formulation elements with reduced integration should be used (see “Hybrid incompressible solid element formulation,” Section 3.2.3, and “Hyperelastic material behavior,” Section 4.6.1 of the Abaqus AnalysisUser's Manual).

When large strain gradients or strain discontinuities are expected in the solution, such as in plasticity analysis at large strains, limit load analysis, or analysis of severely loaded rubber components, the first-order elements are usually recommended. Reduced integration can be used with such elements, but because the hourglass controls are not always effective in severely nonlinear problems, caution should be exercised.

Fully integrated first-order elements should not be used in cases where “shear locking” can occur, such as when the elements must exhibit bending behavior. The incompatible mode elements (“Continuum elements with incompatible modes,” Section 3.2.5 of Abaqus AnalysisUser's Manual) should be used for such applications.

APPENDIX B

B. Bulk Viscosity

(ref..Abaqus 6.11 Analysis User's Manual Vol. II sect. 6.3.3. Dassault Sistèmes)

Bulk Viscosity introduces damping associated with the volumetric straining. Its purpose is to improve the modeling of high speed dynamic events.

There are two forms of bulk viscosity in Abaqus/Explicit.

the first is found in all elements and is introduced to damp the "ringing" in the highest element frequency. This damping is sometimes referred to as truncation frequency damping.

It generates a bulk viscosity pressure (p_{bv1}), which is linear in the volumetric strain:

$$p_{bv1} = b_1 \rho c_d L_e \dot{\epsilon}_{vol} \tag{B.1}$$

where b_1 is the damping coefficient (default=0.06), ρ is the current material density, c_d is the current dilatational wave speed, L_e is the element characteristic length and $\dot{\epsilon}_{vol}$ is the volumetric strain rate.

The second form of bulk viscosity pressure is found only in solid continuum elements (except CPS4R).

This form is quadratic in volumetric strain rate:

$$p_{bv2} = \rho(b_2 c_d L_e \dot{\epsilon}_{vol})^2 \tag{B.2}$$

where b_2 is a damping coefficient (default=1.2) and all the other quantities are as defined for the linear bulk viscosity.

The quadratic bulk viscosity is applied only if the volumetric strain rate is compressive.

The quadratic bulk viscosity pressure will smear a shock front across several elements and is introduced to prevent elements from collapsing under extremely high velocity gradients. Consider a simple one element problem in which the nodes of one side of the element are fixed and the nodes on the other side have an initial velocity in the direction of the fixed nodes. If the initial velocity is equal to the dilatational wave speed of the material, the element - without the quadratic bulk viscosity - would collapse to zero volume in one time increment (because the stable time increment size is precisely the transit time of dilatational wave across the element). The quadratic bulk viscosity pressure will introduce a resisting pressure that will prevent the element form collapsing.

The bulk viscosity pressure is not included in the material point stresses because it is intended as a numerical effect only - it is not considered to be part of the material's constitutive response.

The bulk viscosity pressures are based upon the dilatational mode of each element. The fraction of critical damping in the dilatational mode of each element is given by:

$$\xi = b_1 - b_2^2 \frac{L_e}{c_d} min\,(0, \dot{\epsilon}_{vol}) \qquad \text{(B.3)}$$

Linear bulk viscosity is always included in Abaqus/Explicit. The parameters b_2 and b_1 can be refined by the user. The default values are b_1=0.06 and b_2=1.2. the bulk viscosity parameters can be changed from step to step. If the default values are changed in a step, the new values will be used in any subsequent steps unless they are refined.

Acknowledgements

I would like to thank my Professor, Eng. Enrico Troiani, who trusted me and provided me the opportunity to pursue an advanced learning and to have a truly rewarding experience in Airbus, Germany. He was a strong guide and a point of reference who supported me in all stages of this work from both professional and human point of view.

I'm very grateful to Dr. Domenico Furfari for his mentoring and friendship during my internship in Hamburg. Thanks to him I could develop this project, learning a lot every day. He offered me his insights and encouragement throughout the whole time spent with me and he was a valuable supervisor that I appreciated technically and humanely.

I extend a special thanks to all my colleagues in Airbus who have been particularly kind and made me feel like home.

A deep thanks goes to my "back-up team", Eng. Sara Taddia, Eng. Gianluca Molinari, Eng. Ivan Menghin and Eng. Goran Ivetic, who were always there for precious and constructive suggestions, support and cheering up.

Finally I would like to thank all those people who have helped me directly or indirectly along the path to the completion of this thesis.